5-2010

Mapping a Mutation: Characterization of the ax941 Mutant

Stephen Chi
College of William and Mary

Mapping a Mutation: Characterization of the *ax941* Mutant

A thesis submitted in partial fulfillment of the requirement
for the degree of Bachelor of Science in Biology and Chemistry from
The College of William and Mary

by

Stephen Chi

Accepted for _____
(Honors)

_____
Dr. Diane Shakes, Director

_____
Dr. Mark Forsyth

_____
Dr. Matthew Wawersik

_____
Dr. Robert Orwoll

Williamsburg, VA
April 30, 2010

Table of Contents

Table of Figures

Abstract

Mitosis is a fundamental process shared by all eukaryotes for partitioning DNA into two identical nuclei. In a series of phases, DNA must be properly condensed, aligned, and segregated to give each daughter cell an exact copy of the parental genome. As a failure in mitosis is almost invariably lethal, a plethora of evolutionary conserved molecules exist to regulate and facilitate each step of the process. Among these essential cellular components are histones, nuclear proteins that wind DNA into tightly packed structures known as nucleosomes. Histones are ubiquitously associated with DNA in eukaryotes, and play roles in gene regulation and imprinting in higher organisms. In mitosis, these crucial proteins are responsible for condensing the disordered chromatin into distinct chromosomes, as well as attaching to the kinetochores and microtubules that govern segregation.

In this study, we present our mapping and analysis of the temperature sensitive *C. elegans* mutant (*ax941*) previously described by Mark Astoria (2006) as mutant 1115. The *ax941* mutant was originally isolated by the Seydoux lab in a screen for maternal effect lethal mutations. The maternal effect refers to the preloading of protein products into the embryo by the mother, so whereas mutant males are able to fertilize wildtype hermaphrodites, the fertility of hermaphrodite mutants cannot be restored in crosses with wildtype males. Affected embryos undergo aberrant mitoses, with a range of defects including aberrant DNA segregation during anaphase and delayed telophase often followed by cytokinesis failure. Meiotic divisions are phenotypically normal, but the first mitotic division typically shows errors, with the phenotype fully manifesting by the second or third mitotic divisions. Previous SNP mapping and three-point mapping had placed *ax941* on chromosome I but failed to determine the molecular identity of the mutant. We have subsequently performed additional SNP mapping, deficiency

complementation, and RNA interference experiments in order to determine the gene responsible. Our analysis suggests that the *ax941* mutant gene corresponds to one of two neighboring histone proteins, *his-67* and *his-68*, that form core parts of the nucleosome during early embryogenesis. We propose that since each cell division depletes the quantity of histones available per cell, later cell divisions are unable to properly condense the DNA into distinct chromosomes. Unable to resolve or untangle the interwoven DNA strands, mitosis slows down and a multitude of cellular defects result, producing the variety of phenotypes associated with this mutant. Preliminary sequencing of the two histone genes reveals a potential mutation in the *his-67* gene that changes an alanine residue to a proline residue, a non-conserved change predicted to disrupt the otherwise highly conserved histone structure.

Introduction

Histones

In eukaryotes, mitosis is a fundamental process that divides DNA into identical daughter nuclei in tandem with cellular division. As the loss or gain of DNA can be devastating, both to the cells and the organism, mitosis is heavily regulated by a veritable army of evolutionarily conserved molecules. From cyclins to tubulin to specialized kinases, entire clades of proteins are devoted to delineating and facilitating the distinct phases of mitosis (Doxsey *et al*. 2005, De Clercq & Inze 2006, Walczak *et al*. 2010). Chief among these actors are histones, ubiquitous DNA-binding proteins that condense DNA strands into tightly packed coils. Being intimately associated with DNA at all times, histones play a tremendous role in all aspects of DNA, from transcription and gene regulation in normal cell function, to replication and segregation in mitosis.

Histones are nuclear proteins that structurally organize and control access to DNA. Five distinct classes of histones exist in eukaryotic cells: H1/H5, H2A, H2B, H3, and H4. Of these subtypes, H2A, H2B, H3, and H4 are core histones which make up the core nucleosome – a unit of DNA packaging around which approximately 147 base pairs (bp) of DNA are wound (Kornberg 1974). Two subunits of each core histone are required to form a single nucleosome, creating an octamer of protein subunits with α-helices in the center and DNA-binding loops of amino acids on the outside (Luger *et al*. 1997, Figure 1). The highly modifiable tails of the histones extend outside of the core, and are generally not depicted in nucleosome models due to their structural variability. DNA strands can wind around each nucleosome roughly 1.65 times before detaching. The linker histones H1 and H5 then bind the strands as they separate from the nucleosome, holding up to 80 bp of free "linker DNA" before connecting to another nucleosome

Figure 1. Nucleosome Structure

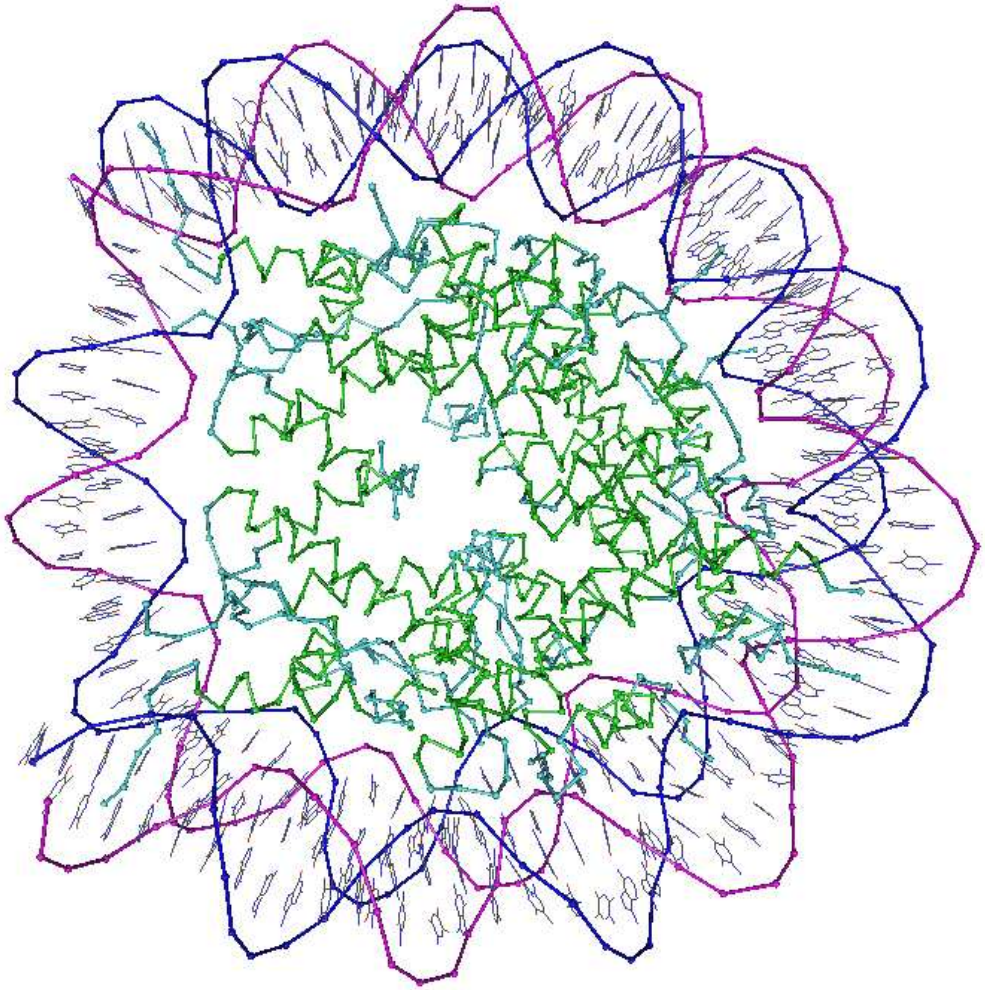

A nucleosome consists of an octamer of histone subunits, around which DNA is wrapped roughly 1.65 times. Histones are shown as green and teal ball-and-stick models in the center; DNA is drawn as blue and purple strands. Histone tails are not depicted due to their extensive post-translational modifications. This structure was created from the hybrid human-*Drosophila* nucleosome structure 2NQB using Cn3D.

(Hasimoto *et al*. 2010). Along with various other DNA-binding proteins, the full ensemble of histones and DNA is collectively known as chromatin (Campos and Reinberg 2009). As histones are tightly associated with DNA, they serve as physical blockers to binding of other proteins, including transcription factors and polymerases. Gene expression and replication therefore requires manipulation of the histones in order to unwind DNA from the nucleosome.

Histones play crucial roles in gene regulation. Eukaryotic genes are traditionally "off" by default, in no small part due to constantly being bound to histones. Decreasing the DNA-histone association leads to a corresponding increase in gene transcription, while increasing the supercoiling can render whole gene clusters silent; entire families of enzymes exist solely to modify histones as part of gene regulation. Acetylation of lysines in the histones' N-terminal tails, for example, lowers the binding strength of histones since the acetyl group neutralizes the positive charge of lysine which ordinarily helps bind the negatively charged DNA strands (Grunstein 1997). Correspondingly, transcription of a gene is necessarily preceded by the recruitment of one or more histone acetyltransferases to grant RNA polymerase access to the DNA. Methylation of lysine and arginine residues, conversely, typically causes even tighter compaction of nucleosomes and represses gene expression. This silencing of gene expression is the fundamental principle of epigenetics, the study of inherited changes in gene expression originating outside DNA's sequence. In combination with the variety of other post-translational modifications that can be performed on histones, including citrullination, phosphorylation, and sumoylation, the variable levels of gene expression dictated by the histones make up the so-called "histone code" of gene regulation (Wilkinson 1987, Xu *et al*. 2009). Since *C. elegans* lacks the ability to silence genes via cytosine methylation, an epigenetic mechanism employed by other eukaryotes, gene cluster silencing typically takes the form of highly condensed

nucleosomes (Simpson *et al*. 1986). Such nucleosome compaction is required not only for epigenetic regulation, but also for cell division.

Segregation of DNA during mitosis requires the coordinated interaction of multiple proteins. As the key structural components of DNA, histones are necessarily involved in DNA movement, yet their functions extend beyond simply holding DNA together while being ferried around. Burgeoning research has identified roles for histones in dictating the location and activity of centromeres – the section of the chromosome where sister chromatids are held together (Allshire & Karpen 2008, Glowczewski *et al*. 2000). The assembly of the proteins that make up the centromere – cohesins and kinetochores – depends on histones as a substrate upon which to bind. As centromeres must subsequently separate neatly to allow the sister chromatids to enter different daughter cells, any disruption of centromere function can lead to improper separation of chromosomes, with severely debilitating consequences (Ahmed *et al*. 2007). Mutations in histones have consequently been linked not only to altered gene expression and regulation, but errors in mitosis and chromosomal segregation as well (Maruyama *et al*. 2006).

Histones compose extensive gene families around each subtype and its variants. Multiple copies of a single histone can be found in a typical eukaryotic genome. No fewer than sixteen copies of the *HIS-30* H2B protein can be found in the *C. elegans* genome, for example, each with an identical amino acid sequence (Wormbase). Note that due to redundancies in the amino acid code, distinct nucleic acid sequences can code for the same protein product. The purpose of having so many gene copies is twofold. Dosage requirements for histones are steep. Consider that the *C. elegans* genome contains 100 million bp, exists in two copies in every cell, and temporarily doubles whenever DNA is replicated. Producing enough histones to organize a genome's worth of DNA in a timely fashion is only possible with multiple copies of the gene

(Ho and Crabtree 2010). The second reason for having numerous gene copies is variable expressivity. The histone requirements are much higher in rapidly dividing cells, such as embryonic blastomeres, than in growth-arrested cells such as neurons. Having several copies of a gene, each of which can be independently activated or repressed, allows for much finer control of how much protein product is made. Histone families also include histone variants, which differ in amino acid sequence and typically serve a specialized role in modifying gene expression. The *htz-1* gene is a variant in the H2B family, for instance, and specifically regulates differentiation of the pharyngeal cells in *C. elegans* (Updike and Mango 2006). Similar cases can be found in all eukaryotes.

C. elegans as a Model Organism

Several features make *Caenorhabditis elegans* an excellent model organism for a wide range of biological studies. *C. elegans* has a generation period of just four days when kept at 20°C; raising the temperature to 25°C can lower the period even further to three days. This short generation time allows laboratory populations to be built up relatively rapidly, and genetic crosses can be completed in swift succession. These crosses are also aided by the fact that *C. elegans* is a hermaphrodite-male species, with the former being self-fertile (Brenner 1974). Each hermaphrodite is capable of producing upwards of a hundred embryos without mating; this considerable brood size can increase to up to three hundred progeny in the presence of males. The adult *C. elegans* body is transparent, allowing researchers to directly visualize development and cellular differentiation, particularly in the prominent gonads. Embryos are likewise relatively large and easy to stain with antibodies and dyes, provided their clear eggshells have been freeze-cracked beforehand. *C. elegans* was also the first species to have its genome fully sequenced, the entirety of which has been annotated and made freely available online at

Wormbase (http://www.wormbase.org). The accessibility and breadth of this database vastly simplifies genetic analysis, both within and across species. A brief BLAST search of the core histones and their associated enzymes in *C. elegans* shows that these conserved proteins closely match human homologs with up to 99% sequence similarity, for example (Altschul *et al*. 1997). Studying mutations in *C. elegans* can therefore yield insights into human biology as well. To this end, a number of temperature-sensitive (ts) mutants have been identified in *C. elegans*. These mutant strains display normal wildtype (wt) phenotypes at low, permissive temperatures, but a mutation in a protein's amino acid sequence causes the protein to become unstable at higher, restrictive temperatures, leading to a mutant phenotype. Since the researcher can consequently control the manifestation of the deleterious phenotype by simply changing the incubation temperature, maintenance of ts mutants in *C. elegans* is trivial. Studying them, on the other hand, demands just as much thought as in any other species.

ax941 Mutant Strain

The *C. elegans* mutant *ax941* is a temperature-sensitive strain that displays abnormal DNA segregation during early embryogenesis. Originally isolated by the Seydoux lab in a screen for ts maternal effect lethal mutants, the *ax941* strain was first characterized by Mark Astoria (2006) in his undergraduate thesis. At the restrictive temperature of 25°C, embryos exhibit a range of defects from the first mitotic cell division onwards (Figure 2): bridging of chromosomes during anaphase, delayed telophase, and abnormal cytokinesis. These mutant phenotypes become more pronounced as embryogenesis continues, with unequal DNA segregation leading to gross differences in DNA content between daughter cells and multiple spindle poles appearing in some cells. All affected embryos die before hatching, and most arrest before even reaching the hundred-cell stage.

Figure 2. *ax941* Mutant Phenotype

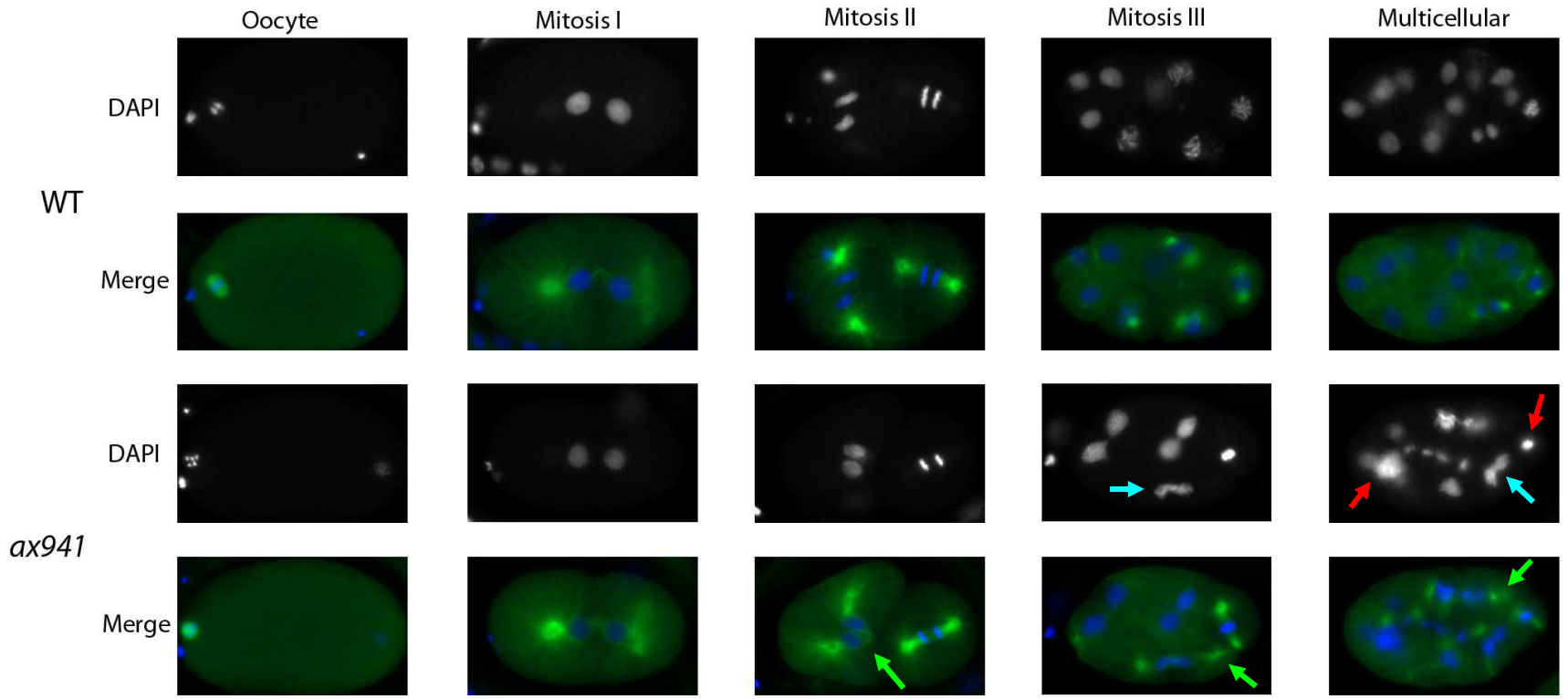

The *ax941* phenotype consists of a plethora of defects, including abnormal DNA bridging during anaphase (light blue arrows), slow telophase, multiple spindle poles, and occasional failure of cytokinesis. Meiotic divisions complete normally, but errors appear as early as anaphase of the first mitotic division and become progressively worse as development continues. Multicellular embryos display markedly unequal nuclear size (red arrows). Tubulin defects are denoted with green arrows. All pictures were taken at 400X optical zoom. DAPI is false-colored blue, tubulin is stained green.

The *ax941* allele is a classic maternal effect mutation. Mutant males are able to successfully fertilize wt hermaphrodites with no visible defects, whereas the fertility of *ax941* hermaphrodites cannot be restored through crosses with wt males. This difference between the sexes implies that the defect is in a maternal product that is preloaded into the embryo in order to facilitate and direct embryogenesis. During early embryogenesis, embryonic transcription is globally repressed until several divisions have passed; maternal mRNA transcripts and protein products instead perform the cellular processes required to synthesize DNA and undergo mitosis (Bowerman 1998). Since the maternal genotype is thus manifested in the offspring's development and phenotype, this phenomenon is termed maternal effect. Maternal effect is common in the development of eukaryotes. In the fruit fly *Drosophila melanogaster*, for example, maternal products are deposited at polar ends of the embryo to create numerous overlapping molecular gradients, which in turn establish body axes and "stripes" of differentiation (Akam 1987). In *C. elegans*, maternal products drive the embryo through the first two mitotic divisions, followed by a transition to a predominantly embryonic transcriptome by the hundred-cell stage (Baugh *et al*. 2003). Since the phenotypic defects of *ax941* are observed during those early mitotic divisions, are specific to the mutant strain's oocytes, and cannot be zygotically rescued by wildtype sperm, we can safely conclude that our defect lies in a maternally deposited gene product.

Mark Astoria's undergraduate thesis work laid the foundations for our present study. Besides establishing the mutant's nature as a maternal effect defect, Astoria also elucidated the limits of the ts phenotype. Meiosis of the oocyte, which completes after fertilization, appeared to be normal. Spermatogenesis likewise demonstrated no obvious defects, with spermatids successfully budding off from the residual body without misappropriation of tubulin or DNA.

Orientation and migration of the sperm and oocyte pronuclei also occurred without incident. The mutant phenotype only arose after metaphase of the first mitotic division, with faulty DNA segregation coincident with aberrant spindles and slow mitotic progression. In order to determine the molecular identity of the *ax941* mutation, Astoria attempted to perform several types of mapping on the locus. Beyond establishing that the mutation lies on chromosome I, however, his mapping was unsuccessful. We have therefore sought to continue his work by mapping the *ax941* mutation and explaining how the plethora of mitotic defects can arise from a single misfolded protein.

Materials and Methods

Strains and Maintenance

The following strains, deficiencies, and markers were used in this study: the Bristol N2 strain as the wt research strain, the CB4856 Hawaiian (HA) strain, *dpy-5 ax941*, *dpy-5; him-8*, *ces-1 qDf5/unc-29 mec-8 dpy-24, ces-1 qDf10/unc-13 lin-11*, and *mnDf111/unc-13 lin-11*.

The *ax941* strain was isolated by the Seydoux lab in an ionizing radiation screen for maternal effect lethal mutants. All strains were stored at 16°C when not in use, and upshifted to 20°C or 25°C incubators as needed. Worms were maintained on agar plates seeded with OP50. Bacterial RNAi strains were stored at -80°C in 80% glycerol, and cultured in LB broth with added ampicillin at 50 μg/ml.

Recombinant Isolation

The SNP mapping of *ax941* was performed on recombinants of a linked *dpy-5 (e61) ax941* strain. To isolate recombinants, *dpy-5 ax941* hermaphrodites were mated to wildtype CB4856 (HA) males, generating *dpy-5 ax941*/HA F1 heterozygotes (Figure 3). F1 non-Dpy hermaphrodites were picked to a fresh plate as L4 larva and upshifted to 25°C. These F1 hermaphrodites were killed 48 hours later, after they had roughly ~100 F2 embryos. From this F2 generation, L4 Dpy hermaphrodites were picked *en masse* to a fresh plate and upshifted to 25°C. Although the vast majority of these F2 Dpy hermaphrodies would have the infertile parental genotype of *dpy-5 ax941/dpy-5 ax941*, rare Dpy hermaphrodites would be fertile *dpy-5 ax941/dpy-5* HA recombinants. Since these F2 plates were kept at the restrictive temperature of 25°C, F2 worms with the parental genotype would fail to leave viable progeny, while fertile recombinant worms would produce F3 progeny. After establishing multiple lines of independently derived recombinant worms, we isolated homozygous recombinant lines by

Figure 3. Recombinant Isolation

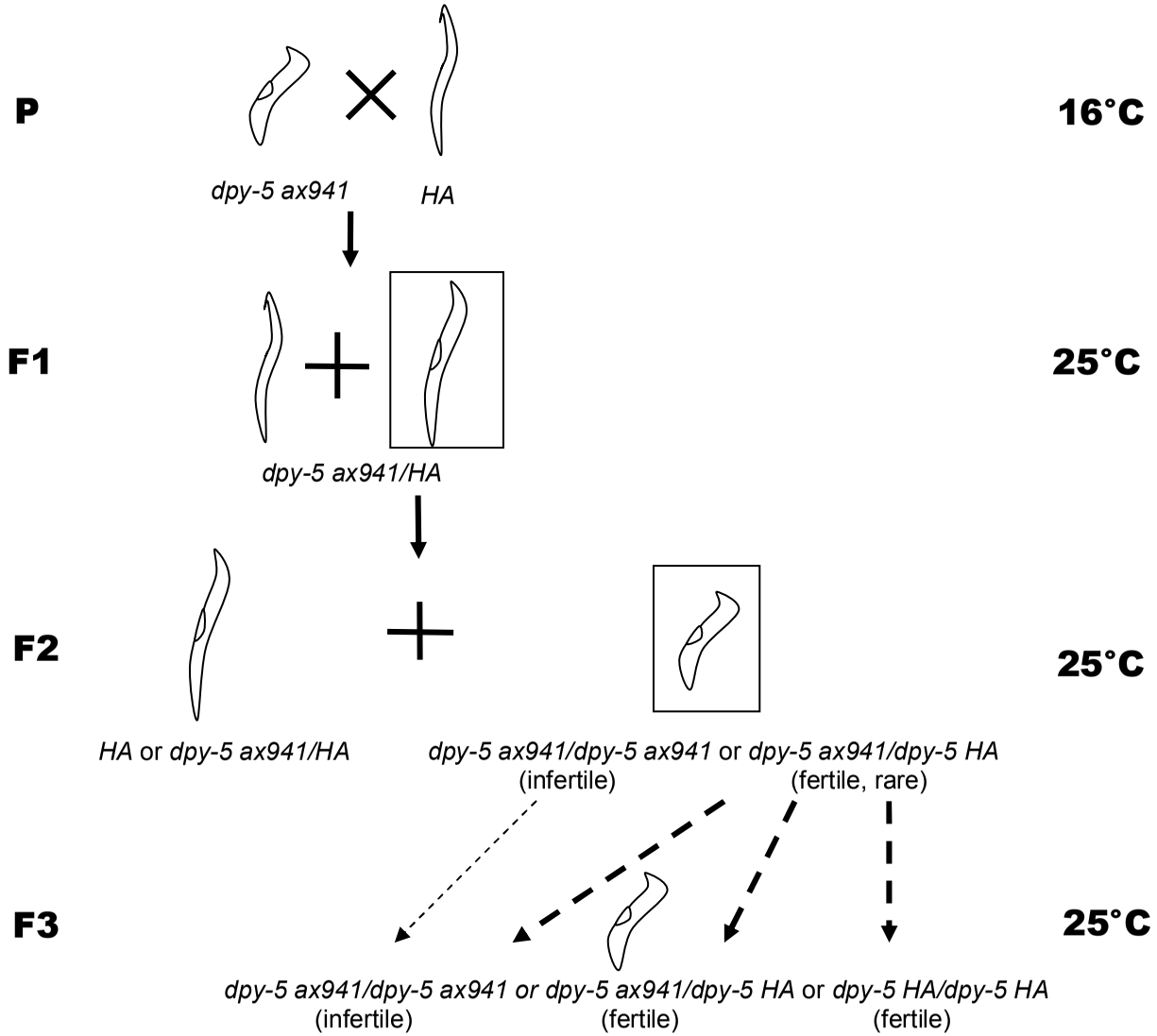

Recombinant lines were generated by crossing *dpy-5 ax941* with HA and selecting for viable Dpy worms. Homozygous recombinants were later isolated from these lines. Male worms are depicted with tail spicules; self-fertile hermaphrodites are shown with vulvas on their bellies; Dpy worms are shorter and fatter than wildtype worms.

picking twelve progeny from single worms to a multiwell plate. Worms that produced 100% fertile progeny at 25°C were scored as homozygous recombinants.

DNA Extraction

We extracted genomic DNA from each homozygous recombinant strain using the 5Prime ArchivePure DNA Cell/Tissue Kit. Worms were washed off the plates using M9 buffer (Brenner 1974), then collected in a 15 ml Falcon tube. After removing excess supernatant, we transferred the worms to an Eppendorf 1.5 ml tube using two 150 µl washes of Lysis Buffer (5Prime). The worms were then sonicated to dissolve the cell membranes, and incubated for thirty minutes with 1.5 µl of 20 µg/µl Proteinase K (Sigma Aldrich). Proteins were removed from solution using 100 µl of Protein Precipitation Solution (5Prime), followed by DNA precipitation using 300 µl of pure isopropanol. To wash, the samples were inverted fifty times in 70% ethanol. Final DNA samples were dissolved in 100 µl of DNA Hydration Solution (5Prime) and stored at -20°C.

Primer Design

Primers for SNiP-SNPs were taken directly from Wormbase if available. For other SNPs lacking a verified primer set, particularly those evaluated by sequencing, primers were designed from the flanking 250 bp region using the Primer3 program (http://frodo.wi.mit.edu/primer3/). Primers were optimized for a length of 20 bp, and a melting temperature of 60°C. All other parameters were left at their default values. Candidate primers were run through BLAST (http://www.wormbase.org/db/searches/blast_blat) to check for multiple annealing positions. If multiple matches were found, non-target matches needed a minimum *e* of 0.1 for the primer to still be considered. For a list of all primers used, see Appendix A. Primers were diluted to 100 µM before usage and stored at -20°C.

PCR

Polymerase chain reactions for SNPs were performed using Promega PCR Master Mix packs. For a 50 µl reaction, we added 25 µl of 2X Master Mix, 2 µl of template DNA, 2 µl each of left and right primers, 5 µl of 10X BSA, and deionized water to volume. Depending on DNA dilution or concentration, we changed these parameters as needed to achieve a better product yield. Typical PCR parameters began with a hot start of 94°C (5 min), followed by thirty cycles of denaturation (30 s), annealing (30 s), and elongation (45 s). Denaturation and elongation occurred at 94°C and 72°C, respectively, while the annealing phase was set to 5°C below the primer melting temperature. Annealing temperatures for all primer sets are listed in Appendix A. A final elongation step at 72°C for seven minutes finished the reaction.

Polymerase chain reactions for gene sequencing were performed using the Roche Expand High Fidelity PCR System. A standard 50 µl reaction contained 0.75 µl of Enzyme Mix, 5 µl of 10X PCR Buffer with $MgCl_2$, 2 µl of template DNA, 2 µl each of left and right primers, 1 µl of 200 µM Nucleotide Mix, and deionized water to volume. PCR parameters were as above, with the substitution of a two minute hot start and a fifteen second denaturation step.

PCR products were evaluated by running a sample in a 2% agarose/TBE gel with ethidium bromide (EtBr) staining. 6X Loading dye was mixed into each sample as appropriate before loading, and a 100 bp DNA ladder was used to evaluate band sizes. Gels were imaged using a Bio-Rad Fluorescent Imager, using the Quantity One software. If the PCR product was to be used in direct sequencing, then the entire sample was loaded into the gel, and the DNA band was subsequently extracted and purified using the Qiagen Gel Extraction Kit protocol. Final DNA concentrations were determined using a Nanodrop Spectrophotometer (Fisher Scientific), using the Nucleic Acid protocol.

Sequencing

Sequencing was performed by the Molecular CORELab at the College of William and Mary, following their protocol. Each submitted sample contained 20-100 ng of DNA and 0.5-5 picomols of primer in 8 µl of solution. Sequencing results were analyzed using BioEdit (http://www.mbio.ncsu.edu/BioEdit/bioedit.html).

Enzyme Digests

Enzyme digests of SNiP-SNPs were performed using the respective restriction enzymes listed on Wormbase and purchased from Promega. A standard enzyme digest of 20 µl contained 2 µl of enzyme buffer, 2 µl of DNA, 0.2 µl of 10X BSA, 5 µg of restriction enzyme, and deionized water to volume. Reaction tubes were incubated at 37°C for two hours, and then upshifted to 70°C for twenty minutes to halt the reaction. Digested samples were stored with 6X loading dye at 4°C before being evaluated in a 2% agarose gel with ethidium bromide staining.

Deficiency Complementation

Since homozygous deficiency worms are inviable, genetic crosses must be performed on heterozygous deficiency worms with balancer alleles on the opposite chromosome. Deficiency strains were ordered from the *Caenorhabditis* Genetics Center at the University of Minnesota. To perform a deficiency cross, we crossed homozygous *dpy-5 ax941* hermaphrodites with heterozygous deficiency/balancer males at 16°C. On each subsequent day, the resulting embryos were shifted up to the restrictive temperature of 25°C. If the chromosomal deficiency complemented the *ax941* locus, then the F1 progeny would be *ax941*/wt at the *ax941* locus. If the chromosomal deficiency deleted the *ax941* locus, conversely, then the F1 progeny would be *ax941*/null at the mutant locus and would exhibit the mutant phenotype (Sigurdson *et al*. 1984,

Figure 4. Deficiency Crosses

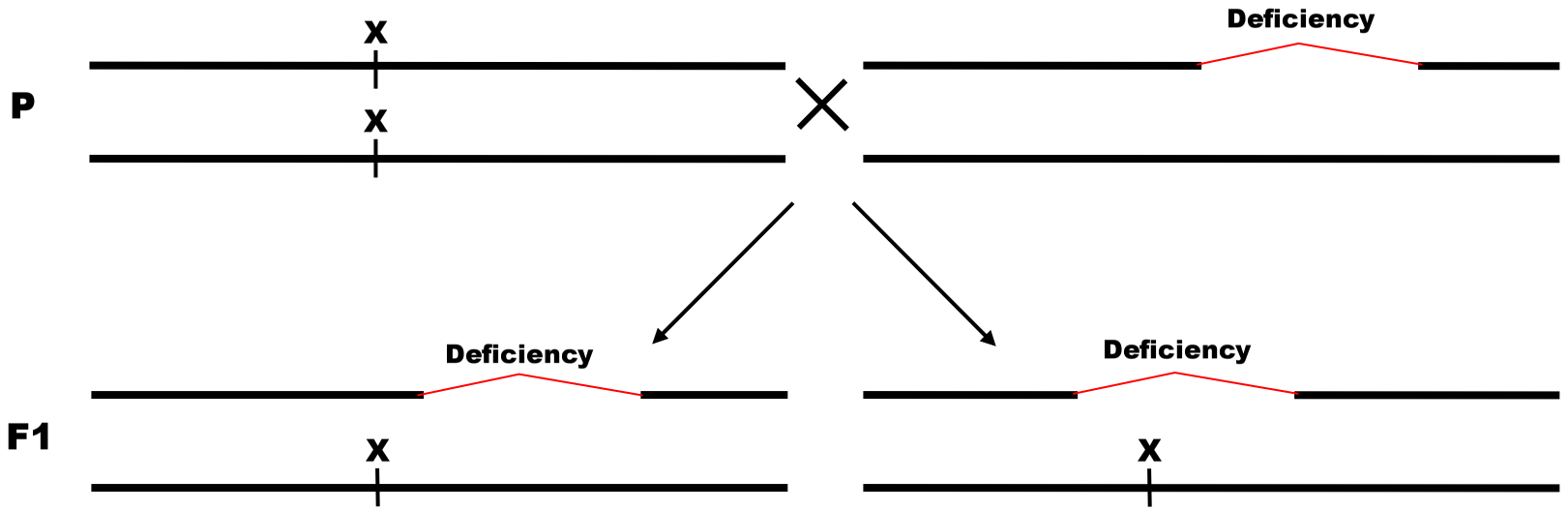

Deficiency crosses can have two possible results. If the deficiency complements the mutation, as seen on the left, then the recessive mutation will not emerge in the F1 generation. If the deficiency deletes the locus of interest, as shown on the right, then the monoallelic X locus will cause the mutant phenotype to arise in the F1 generation.

Figure 4). Deficiency crosses with predominantly dead embryos were scored as failing to complement the *ax941* locus.

RNA Interference

RNA interference (RNAi) was performed using bacterial lines from GeneService's *Caenorhabditis elegans* RNAi feeding library (Timmons & Fire 1998, Fraser *et al*. 2000). To generate RNAi cultures, single colonies were picked from each line for RNAi cultures. Cultures were grown overnight at 37°C in LB broth with ampicillin added to a concentration of 50 μg/ml. Agar plates were prepared with 0.5 mM IPTG and 50 μg/ml ampicillin; 125 μl of liquid culture was seeded onto each plate. Worm strains used were wildtype N2 and *ax941; him8*. N2 plates were kept at 25°C to improve RNAi penetrance. To provide a sensitized background, RNAi was also performed in the *ax941; him8* strain at the normally permissive temperature of 20°C. Approximately eight L4s or ten L1s were picked to each plate and transferred to fresh plates after one day of laying embryos. Embryonic lethal phenotypes were scored by the persistence of dead embryos on the plate in the presence of bacteria. Each line was evaluated in a minimum of two independent runs with five or more sets of replica plates.

Dissection and DAPI/α-Tubulin Staining

To dissect the worms, we prepared Fisher Brand Color Frost Plus slides with evaporated poly-L-lysine for additional positive charge. Adult worms were transferred to 12 μl of egg buffer containing 4 mM levamisol as a paralyzing agent (Boyd *et al*. 1996). We dissected embryos from the adults using a midway cut from a 27.5 gauge needle. After slightly squashing the embryos with a coverslip, we immediately freeze cracked the eggshells in liquid nitrogen and fixed the embryos in -20°C dry methanol overnight.

Immunostaining of the embryos began with three five-minute washes of phosphate buffer solution (PBS) to remove methanol and other impurities. A twenty-minute blocking phase then followed, using PBS with added 0.5% BSA and 0.1% Tween. We subsequently incubated the slides with 1:100 diluted FITC-conjugated anti-α-tubulin monoclonal antibody (Sigma Aldrich, DM1A) for two hours in a humidity chamber to prevent drying out. After incubation, the slides were dip-washed in PBS and dried using a Kimwipe. A drop of mounting media with 1 μg/ml 4',6-diamidino-2-phenylindole was applied to the slide, followed by final addition of a coverslip. Slides were stored at 4°C in a covered folder.

Slides were viewed using an Olympus BX60 microscope mounted with a SensicamQE (Cooke Corporation). IPLab software was used to capture and save images, which were then formatted in Adobe Photoshop CS4 as needed.

Results

Our mapping of the *ax941* mutation has taken a tripartite approach: single nucleotide polymorphism (SNP) mapping, deficiency mapping, and RNA interference. As the three techniques differ substantially in scale, specificity, and data yielded, they have allowed us to progressively narrow the candidate region from the length of a chromosome to individual genes. This multifaceted approach has provided independent corroboration of specific findings, improving confidence in our data. Previous SNP and three-point mapping by Mark Astoria had found that *ax941* was located on chromosome I, but his exact mapping results were highly conflicting. Working in conjunction with researchers at Virginia State University, we therefore sought to refine Astoria's results, beginning with SNP mapping the *ax941* mutation.

SNP Mapping

Single nucleotide polymorphism mapping is a powerful mapping protocol for cloning genes (Davis and Hammarlund 2006). The technique is particularly suited to *C. elegans* research due to the existence of two distinct, well-studied strains: the canonical N2 (Bristol) strain from England, and the CB4856 strain from Hawaii, abbreviated HA. The N2 and HA strains have been separated for a sufficient evolutionary time period that a number of SNPs have become fixed between the two genomes. Since research in *C. elegans* began, many of these SNPs have been documented and made publically available for reference in Wormbase (http://www.wormbase.org). This divergence causes slight phenotypic effects, but not enough to create a reproductive barrier. Mating between the strains consequently occurs readily to produce progeny with distinct HA and N2 DNA. Even if the genomes are further recombined via crosses, a researcher can determine the origin of any length of DNA simply by examining the SNPs where recombination has occurred.

SNP mapping is a complex extension of standard three-point mapping (Fay 2006). Traditional three-point mapping compares the frequency of recombination between the gene of interest (X) and two marker genes (A and B) (Figure 5). Consider a heterozygote strain that contains X on one strand and A and B on the other, flanking X's genetic position. By chance, recombination between the strands at a site between A and B will create progeny that possess X and either A or B. The frequency at which these A non-B and B non-A strains arise in relation to each other depends on the distance between X and the marker gene: if A and X are far apart, then recombination to form an A non-B progeny has a higher chance to occur than if the two were close together. The same holds true for B, allowing the researcher to make the following critical comparison. Assuming an equal rate of recombination along the established genetic map, the relative frequencies of A non-B and B non-A recombinants are equal to the relative distances of X to A and B, respectively. A 50:50 ratio of A non-B to B non-A recombinants suggests that X is halfway between A and B, for instance, whereas a 90:10 ratio would imply that X is located nine times closer to B than A. With the ability to determine genetic locations with high certainty, three-point mapping has long been the mainstay of genetics in *C. elegans*. SNP mapping expands this technique by employing nearby SNPs as genetic markers to repeatedly narrow down the location of X, vastly increasing the resolution of the mapping.

SNP mapping analyzes the SNPs of multiple independent genetic recombinants to establish an absolute boundary on a gene's location. Suppose that in the first step of three-point mapping described above, the heterozygote strain had been formed from a cross of N2 and HA parents. On an experimental level, this protocol assumes the gene of interest X and the marker genes A and B were isolated in different *C. elegans* strains; in convention with traditional *C. elegans* research, assume X was found in N2 while A and B came from HA. The recombination

Figure 5. Three-Factor Crosses

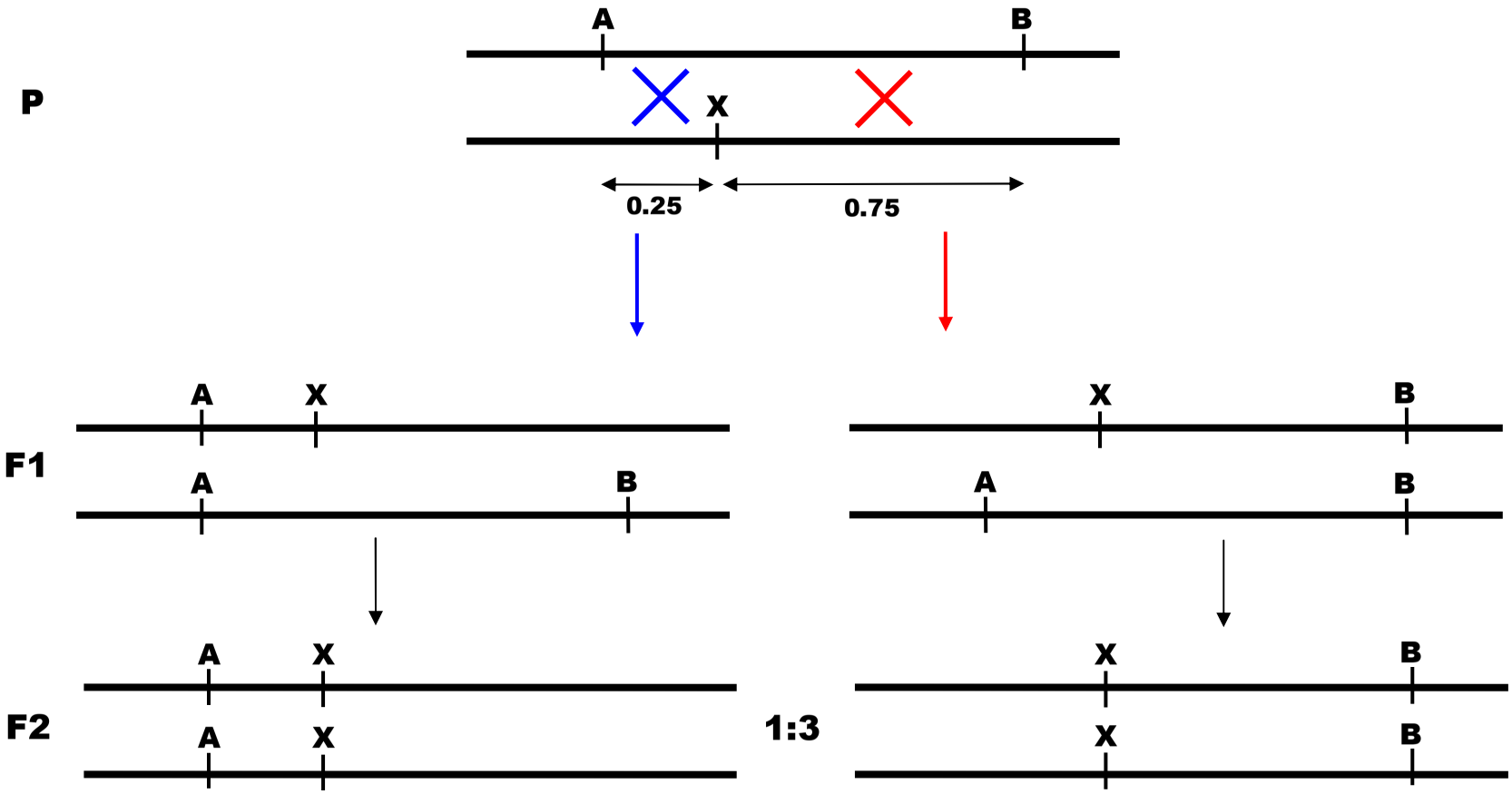

Three-factor crosses between two marker genes and a gene of interest yields A non-B and B non-A recombinants in proportion to the distance between A, B, and X. In this example, the genetic distance between B and X is three times greater than the distance between A and X, leading to three times as many B non-A recombinants in the F2 generation.

step would then create a hybrid strand of DNA, consisting of N2 DNA at the end with X, and HA DNA at the end with A or B. The site of recombination would therefore be defined by the transition from N2 to HA DNA, which a researcher would deduce by documenting the parental DNA of origin for known SNPs between A and B. This process yields two crucial pieces of mapping information (Davis and Hammarlund 2006). The first results from the fact that X must be located on N2 DNA in every recombinant. So out of all the recombinants sampled, the SNPs furthest from A and B that possess HA identity in any of the samples must represent definite endpoints for X's location. Whereas three-point mapping can only yield a position relative to the marker genes used, SNP mapping gives the researcher a conclusive limit to X's possible location dependent only on the SNPs sampled. The second piece assumes that the rate of recombination varies linearly between the marker gene and X. In an A non-B recombinant, the rate of recombination must be 100% at A, but 0% at X. In other words, SNPs near A would exhibit HA DNA almost exclusively, whereas SNPs near X would show predominantly N2 identity. If recombination indeed correlates linearly with distance, then a SNP halfway between A and X would therefore match N2 DNA in half the recombinants and HA DNA in the other half; similarly, a SNP located three-fourths of the way to X would identify with N2 DNA in roughly three out of every four recombinants. Plotting genetic distance against recombination rate theoretically generates a straight line, with the location of X at the point where the recombination rate is 0%. SNP mapping both restricts and predicts the location of a gene of interest.

While our experimental protocol differed slightly from the theory established above, the general principles remained the same. We notably did not perform three-point mapping with two marker genes on either side, instead using a single marker and data from SNPs alone for our first experiment. We also started with a *dpy-5 ax941* N2 strain. The *dpy-5* marker, which induces a

short, “dumpy” (Dpy) phenotype (Thacker *et al*. 2006), was originally crossed into the strain to facilitate identifying *ax941* at permissive temperatures of 20 °C or below. Fortunately for our experiment, this linked strain also allowed us to perform the reverse of a standard recombination experiment: instead of selecting for recombinants that kept the mutation and gained a marker gene, we screened for recombinants that lost the mutation but retained the marker gene (Figure 6). Conceptually the experiment was the same, with the exception that the recombination rate would be 100% at the site of *ax941* and 0% at the marker gene.

Our procedure followed standard recombinant isolation steps, with additional considerations for the temperature sensitivity of *ax941*. To isolate recombinants, we first crossed *dpy-5 ax941* homozygous N2 hermaphrodites with wildtype (wt) HA males at 20°C, generating *dpy-5 ax941*/HA heterozygous hermaphrodites with a wildtype phenotype, among others. Of those heterozygous F1 worms, we picked hermaphrodites and upshifted them to 25°C to increase the frequency of meiotic recombination in their gametes. As expected, roughly a quarter of their progeny displayed the *dpy-5* phenotype. To screen these F2 worms for recombination between *dpy-5* and *ax941*, we picked any *dpy-5* worms and allowed them to mature at 25°C: *dpy-5 ax941/dpy-5 ax941* non-recombinants would fail to produce to progeny in accordance with the *ax941* phenotype, whereas *dpy-5 ax941/dpy-5* F2 worms heterozygous for HA DNA at the *ax941* locus would survive (Figure 3). We assumed that no more than one desired recombination event occurred for each plate of F2 worms. Out of approximately sixty potential recombinants, we isolated twenty independent homozygous recombinant lines from which we extracted genomic DNA.

Our next step was to PCR amplify select SNPs between *dpy-5* and *ax941*’s presumed location. Primers for each selected SNP were taken from Wormbase if verified PCR products

Figure 6. *ax941* SNP Mapping

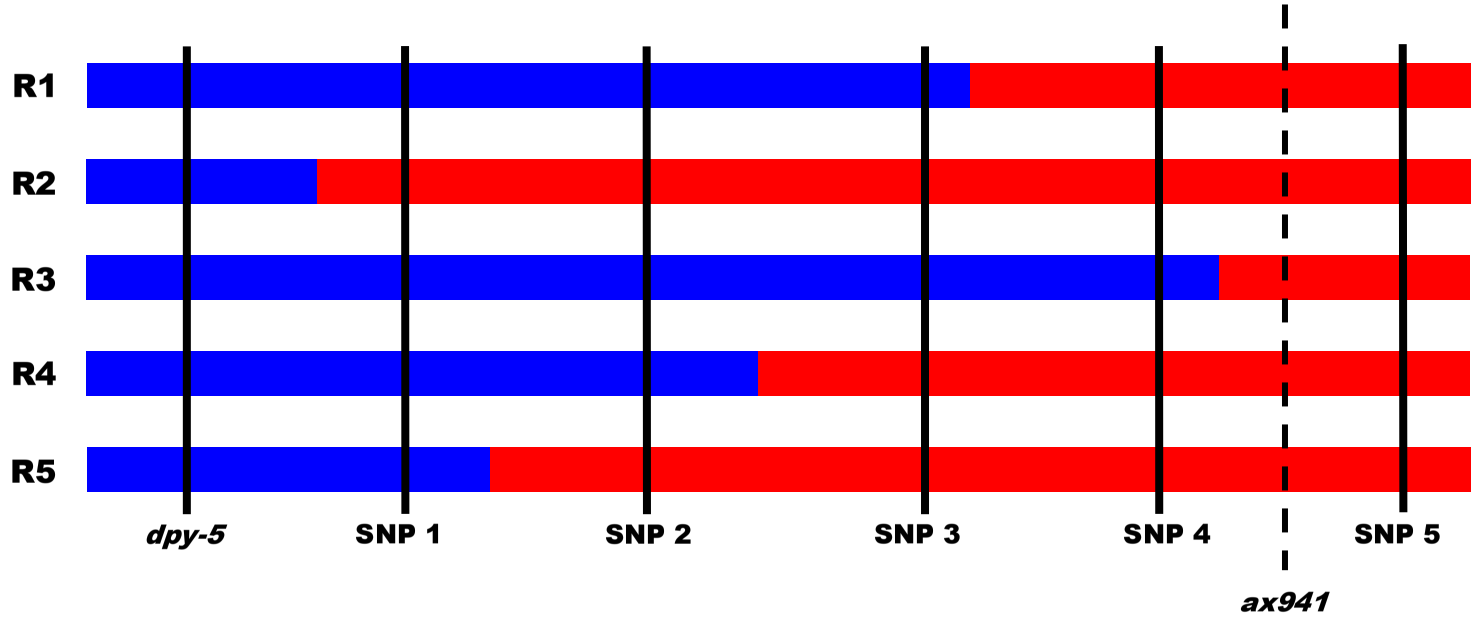

	Locus					
Recombinant	***dpy-5***	**SNP 1**	**SNP 2**	**SNP 3**	**SNP 4**	**SNP 5**
R1	N2	N2	N2	N2	HA	HA
R2	N2	HA	HA	HA	HA	HA
R3	N2	N2	N2	N2	N2	HA
R4	N2	N2	N2	HA	HA	HA
R5	N2	N2	HA	HA	HA	HA
Rec. Rate	0%	20%	40%	60%	80%	100%

In this idealized example of SNP mapping, five recombinant lines have undergone a recombination event between *dpy-5* and *ax941*, leading to HA DNA at the *ax941* locus. Plotting the recombination rates against the genetic locations of SNPs 1 through 4 would give a predicted location of *ax941*. Note that SNP 5 is excluded from analysis since a recombination rate of 100% could correspond to any point from just before *ax941* to anywhere past the locus. Since SNP4 is the last SNP to have N2 DNA in one of the recombinant lines, its genetic location is an absolute boundary for *ax941*'s location.

were available. If confirmed primers were not available, we constructed primers from the flanking regions using the Primer3 program (http://frodo.wi.mit.edu/primer3/), optimized for 20-21 nucleotides and 60 °C melting temperature. All primers were checked in BLAST to test for multiple annealing points; for all other sequences in the genome with a partial match to the primer, a minimum *e* value of 0.1 was required. Our colleagues at Virginia State University had previously performed SNP mapping using another marker gene at *unc-101*, which is located at map position 13.23 on chromosome I. Their results were inconclusive, however, with results that placed *ax941* within a range of several million base pairs far to the left of *unc-101* (unpublished data). With this knowledge, we selected SNPs that covered an area roughly halfway between *unc-101* and *dpy-5*, which is situated at map position 0.0. For a list of these SNPs, see Table 1. For ease of testing, we chose SNPs that caused restriction fragment length polymorphisms, commonly called SNiP-SNPs. All SNiP-SNPs were digested with the respective enzymes documented in Wormbase for a minimum of 2 hours at 37 °C. Since these SNPs exhibited different cutting patterns between N2 and HA DNA, we could obtain our results simply by running a gel, rather than costly sequencing. From this first batch of SNPs, we obtained the results shown in Figure 7 and summarized in Figures 8 and 9.

This experiment succinctly demonstrates the potential of SNPs for mapping genes. After determining the identity of each SNP in all twenty recombinant strains, we calculated the recombination rate at each SNP by dividing the number of HA-displaying strains by the total number of strains. Plotting this fraction against the genetic position of each SNP yielded Figure 8. The first point of notice is that only SNPs with a recombination rate below 100% were used in the analysis. As stated earlier, because of our altered protocol, the theoretical location of the *ax941* mutation is the point at which the recombination rate first reaches 100%. SNPs that

Figure 7. Enzyme Digests of SNiP-SNPs

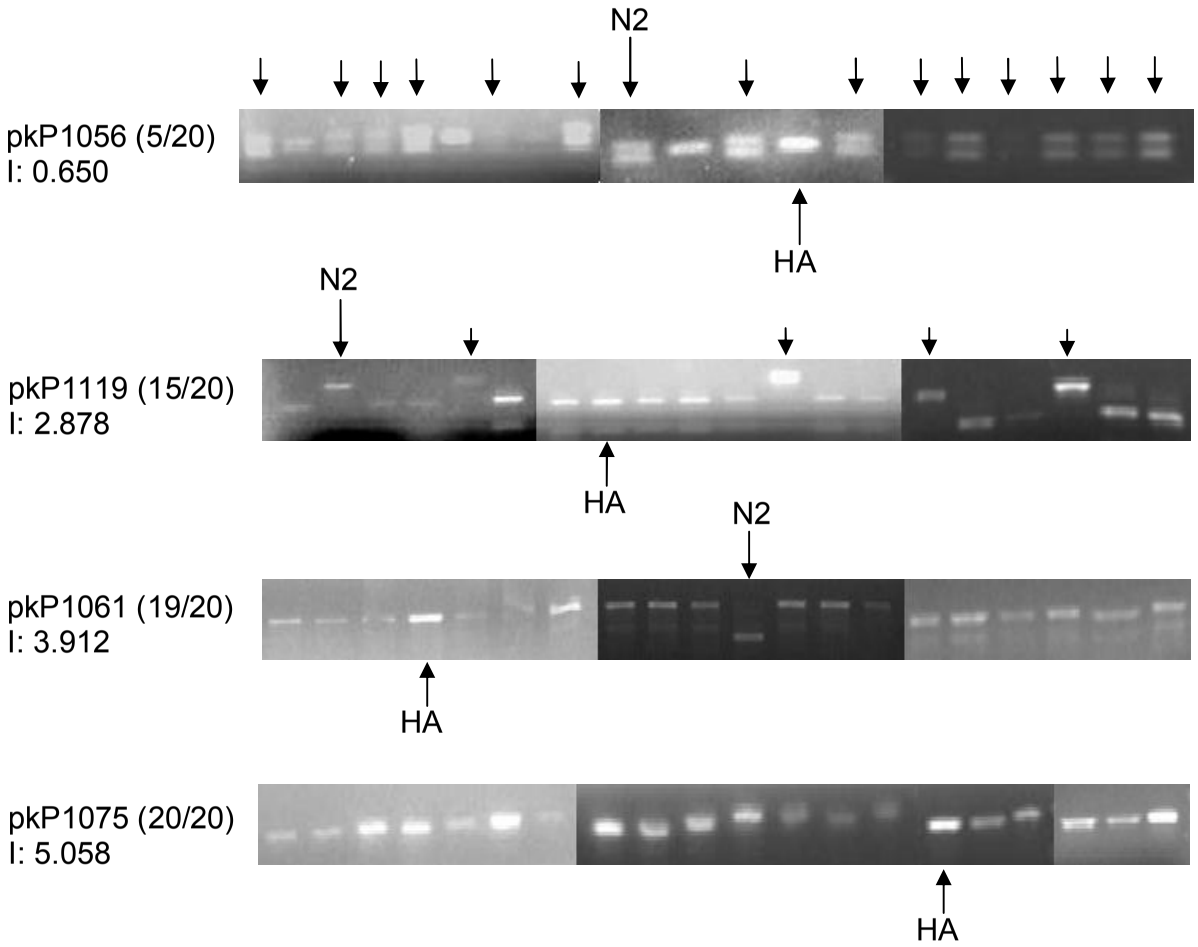

Enzyme digests of the four initial SNiP-SNPs yielded useful data for three SNPs. SNiP-SNPs cut N2 and HA DNA differently because the SNP adds or removes a restriction endonuclease recognition sequence, allowing us to evaluate the DNA's identity from the unique banding patterns. Each lane represents a different recombinant line. The ratio in parentheses is the proportion of recombinants showing HA DNA at that SNP.

Figure 8. SNP Mapping Results

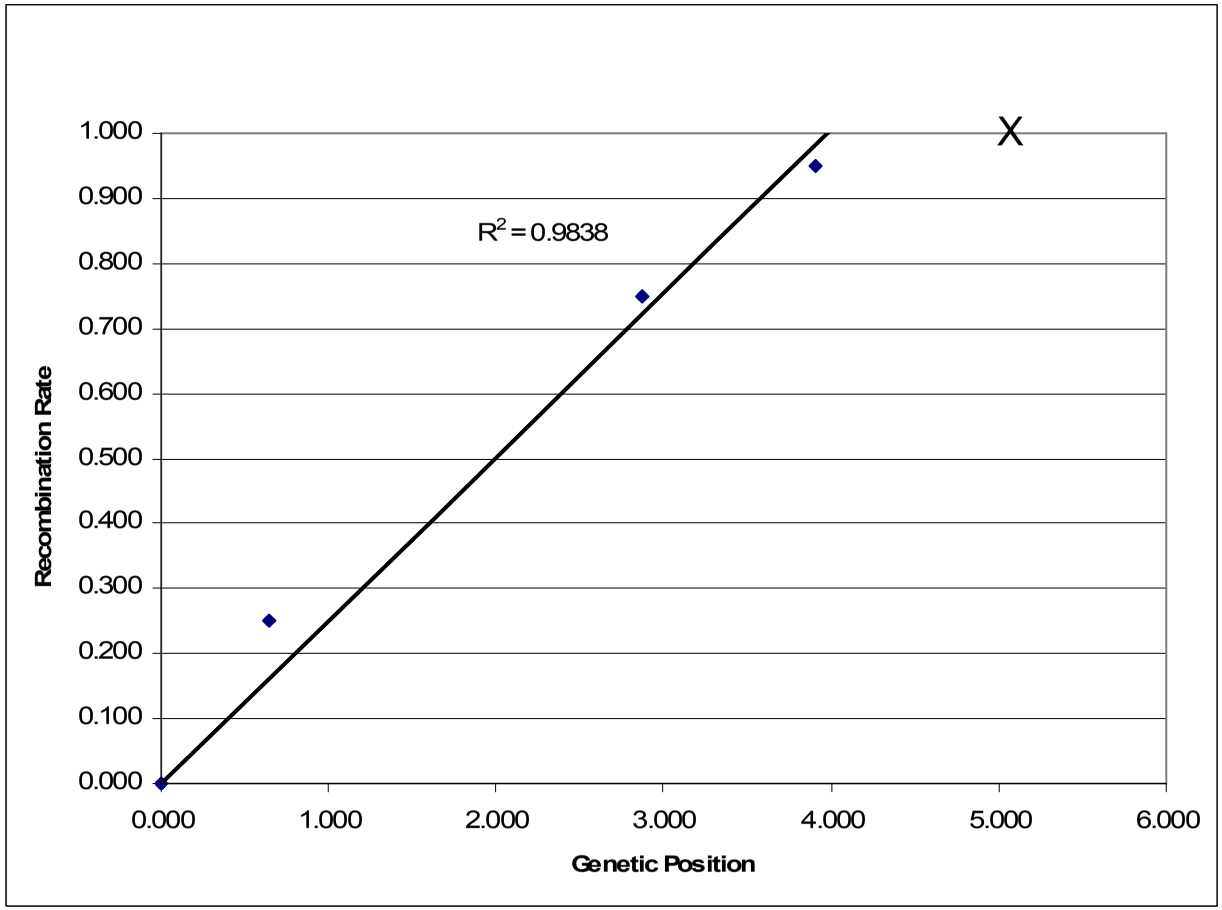

Analysis of three SNPs between *dpy-5* (0.0) and *ax941* produces a nearly linear fit that predicts *ax941* to be located at map position 4.1. A fourth SNP at 5.056 was excluded from the regression.

Figure 9. Mapping Summary

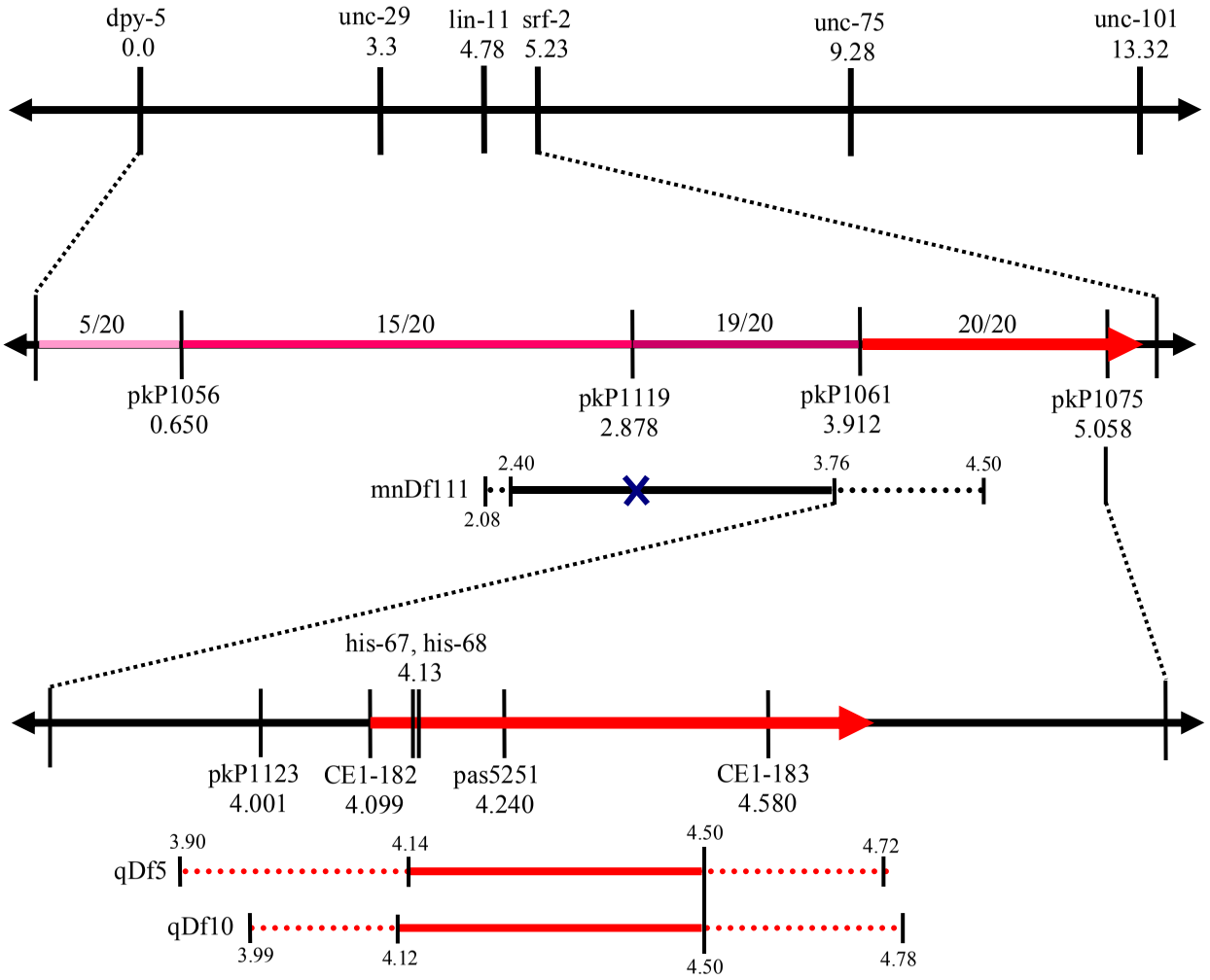

Our SNP and deficiency mapping gave a leftward boundary of 4.099 and a rightward boundary of 4.72 for the *ax941* locus, with a higher likelihood of lying to the left. Although *pas5251* initially directed our mapping to the right, we subsequently ignored this SNP on the basis that a gene conversion event likely took place.

display a recombination rate of 100% are consequently uninformative, as they represent SNPs that can be either right before or any distance past the gene's location. Since *pkP1075* had a recombination rate of 100%, as denoted by the X, its data was discarded from our discussion. Nevertheless, despite covering an distance of approximately four million base pairs between them, the other three SNPs provided an excellent estimate for the location of *ax941*. The rightmost SNP of the three, *pkP1061*, provided our first boundary of *ax941*, vastly limiting our search area to the right of 3.912. With the other SNPs, we then constructed a linear regression to predict *ax941*'s location. As seen in Figure 9, the calculated site was at roughly 4.1 map units. We subsequently tested additional SNPs in order to further elucidate the location of *ax941*.

After ordering additional SNP primers, we continued our mapping with mixed results. With only one of our twenty recombinant lines showing N2 DNA at *pkP1061*, we focused our attention on this one strain, hoping to push the left boundary further to the right. The tested SNPs are listed in Table 2. With a target area of 4.1 map units, we predicted that SNPs *pkP1123* (4.001) and *CE1-182* (4.099) would both show N2 DNA, while *pas5251* (4.240) and *CE1-183* (4.580) would exhibit HA DNA. Note that even if the former two SNPs identified with HA, such a result would only indicate that recombination occurred to the left of our estimated position. We instead found N2 DNA at *pkP1123*, *CE1-182*, and *pas5251*, which pushed the boundary for *ax941*'s location to 4.240 (Figure 9). *CE1-183* did show HA DNA, but that result did not necessarily rule out *ax941* being even further to the right. We had to consider several caveats, however. With only one strain to test on, any results must be taken with a heavy grain of salt, since we had no way of corroborating these findings. Furthermore, *pas5251* is only a predicted SNP of adenine repeats, which are notorious for being faulty reads. We subsequently sequenced the *pas5251* region in HA, N2, and *ax941* strains in order to determine whether the

pas5251 SNP actually existed. All findings pointed to *pas5251* being a real polymorphism. Our SNP mapping therefore placed *ax941* to the right of 4.240 on chromosome I, with a high likelihood of being near that boundary as predicted by the linear regression.

Deficiency Mapping

With this initial finding in hand, we sought to verify our SNP mapping results with an independent mapping protocol. Deficiency mapping is an easily performed mapping procedure that comes at the cost of some experimental certainty. Using ionizing radiation or chemical treatment, sections of chromosomes can be removed from an organism's genome. Numerous strains of *C. elegans* have been created with these so-called deficiencies, varying in size and location to collectively cover the entire genome (Sigurdson *et al*. 1984). These strains are maintained as heterozygotes with balancer mutations on the other chromosome, as individuals missing both copies of the deficiency are generally inviable. Even heterozygote strains typically suffer in fitness due to insufficient gene dosage, leading many deficiency strains to spontaneously fall apart without proper maintenance. Characterization of deficiency strains has been historically inconsistent as well, with the breakpoints of the deficiency often vaguely defined in terms of genes known to be inside or outside. In some cases these genes are hundreds of thousands of base pairs apart, leading to substantial difficulties in interpreting any results. The upside is that deficiency mapping is an efficient means of obtaining left and right boundaries of recessive mutations. Crossing a recessive mutant strain with any other strain normally leads to wildtype F1 progeny that are heterozygous for the mutation. If the deficiency deletes the locus of interest, however, then a predictable fraction of the progeny from a deficiency strain crossed to the mutant strain will inherit just the mutated allele and no complementary DNA from the other parent. That progeny would then be effectively monoallelic at the gene of interest, and

therefore display the recessive phenotype in the F1 generation (Figure 4). The boundaries of the gene of interest would then be given by the breakpoints of the deficiency. Deficiency mapping thereby serves as a quick, if somewhat unstable, means of mapping recessive mutations in a variety of species (McKim *et al*. 1992, Ionine *et al*. 2002, Dai *et al*. 1999).

For our experiment, we tested several deficiencies around the site predicted by our SNP mapping. Astoria had previously attempted to do the same experiment, but obtained wildly varying results. Later examination of his strains revealed breakdowns in some of his deficiency strains. We consequently sought to repeat his experiment using three deficiency strains as described in Table 2: *qDf5*, *qDf10*, and *mnDf111*. Two of these deficiencies, *qDf5* and *qDf10*, were chosen since they cover the area predicted by our SNP mapping. The last deficiency, *mnDf111*, was selected in order to verify the 4.240 boundary established by our SNP mapping. Our results were exactly as expected: *qDf5* and *qDf10* crosses showed the *ax941* phenotype in some of the F1 progeny, whereas *mnDf111* crosses retained full fertility at 25°C (Figure 9). We therefore corroborated our SNP mapping results and further obtained a right boundary of 4.72 for the *ax941* mutation. With the *ax941* mutation firmly boxed in on either side, we moved on to testing individual genes.

RNA Interference

RNA interference (RNAi) is a powerful technique for silencing translation of specific genes (Fire *et al*. 1998). Silencing RNA (siRNA) employed in the laboratory mimics the natural microRNA (miRNA) system used by *C. elegans* and many other eukaryotes to post-transcriptionally regulate gene expression. Consisting of just 20-22 nucleotides on average, miRNAs are non-coding RNAs that have been conserved over evolutionary history for their ability to silence entire groups of related genes (Lim *et al*. 2003). By binding to the 3' UTR of

genes' messenger RNA, they form double-stranded RNA complexes that are subsequently processed and cleaved, effectively halting translation of those genes. siRNA exploits this regulatory process to target not gene clusters, but single genes. By using synthetic double-stranded RNA (dsRNA) that matches the specific 3' UTR of the target gene, RNAi can sever the expression of one gene while leaving others unaffected (Fire *et al*. 1998, Pushparaj *et al*. 2008). This "knock down" effect is theoretically similar to the decreased gene expression caused by a mutated gene. We therefore sought to identify the *ax941* mutation by knocking down genes one by one until a similar phenotype was found.

In theory, the process of introducing dsRNA for RNAi in *C. elegans* is nearly trivial. Simply bathing the worms in a solution containing the dsRNA, for example, is sufficient for some cells to uptake and process the silencing RNA. The worms may alternatively be fed bacteria that have been transformed with a plasmid expressing the sequence of interest, along with an appropriate operon of choice. We chose the latter method for its relative ease and reliability compared to injection and bathing techniques. Dr. Aurora Kerscher graciously provided GeneService RNAi bacterial clones for our experiments. These bacteria contain a plasmid with a specific gene sequence paired to the *lac* operon. The *lac* operon normally controls expression of *β*-galactosidase, used in the metabolism of lactose; the presence of lactose or its metabolites acts as an inducer for expression of the entire operon. Isopropyl *β*-D-1-thiogalactopyranoside (IPTG) is a substance that mimics allolactose, an intermediate of lactose metabolism that activates the *lac* operon. Unlike allolactose, however, IPTG cannot be hydrolyzed. Placing IPTG in our agar plates consequently led to the constant activation of the *lac* operon in these bacteria, which then produced the desired RNAi substrate. Subsequent feeding of these bacteria to the worms introduced the dsRNA to the worm's cells.

In practice, the analysis of RNAi phenotypes in *C. elegans* has several caveats (Maine 2008). Whereas a researcher can clip off the end of a mouse's tail to measure the level of RNAi in the entire organism, quantifying genetic knock down in *C. elegans* is nearly impossible. The penetrance of RNAi varies markedly from worm to worm and from gene to gene, leading to RNAi phenotypes that typically appear in only a portion of tested worms. Other genes display no RNAi phenotypes whatsoever despite having a functional role; these genes may have genetic redundancies, or affect fitness only under certain circumstances, e.g. high temperature or starvation. The last concern surrounds the fact that "knock down" may not necessarily reflect a ts mutant's molecular phenotype. Since the *ax941* mutant is temperature-sensitive, the most likely molecular cause is a protein rendered thermally unstable by a change in amino acid sequence. Raising the temperature therefore depletes the levels of functional protein in the cell by unfolding the protein's structure. In contrast, RNAi depletes the levels of functional protein by either destroying or halting translation of the mRNA. While both phenotypes may be described as insufficient dosage of protein, a ts mutant may still have partially functioning or non-functional proteins in the cytoplasm. Although these misfolded copies should theoretically be degraded by cellular chaperones, leading to a full loss-of-function, in some cases the faulty protein engages in additional activity that exacerbates the mutant phenotype. Complex poisoning, for instance, occurs when mutated proteins not only lose their function, but prevent their binding partners from acting as well. These cases are relatively rare, however, and an insufficient dosage of functional protein does explain most ts mutant phenotypes. Keeping these considerations in mind, we therefore sought to replicate the *ax941* mutant phenotype in both wildtype and mutant strain worms using RNAi.

Our RNAi experiments yielded data that conflicted with our SNP mapping results. We began our RNAi tests after obtaining the data shown in Table 1 and Figure 8, choosing twelve genes between 4.1 and 4.5 (Table 4). These twelve comprised almost all of the genes located in the chromosomal interval, with the exception of spermatogenesis-enriched genes and RNA genes (e.g. miRNAs, 21-U RNAs). We first scored for embryonic lethal phenotypes, followed by dissection and staining. Of those twelve genes, *his-68* produced dead embryos, and our preliminary dissections showed that *his-68* knockdown strongly resembled the *ax941* phenotype (Figure 10). Since *his-68* is located at 4.13, this finding directly contradicted the SNP mapping result that the locus had to be to the right of 4.24. Resolving this discrepancy between RNAi and SNP mapping quickly became the focus of our research.

Determining the location of the *ax941* locus required careful weighing of our SNP mapping and RNAi results. Sequencing of the predicted SNP at 4.240, *pas5251*, had provided strong evidence that the variation existed between the HA and N2 strains. Subsequent sequencing of the recombinant strain also showed that the strain's genomic DNA definitively matched the N2 form of the polymorphism. We consequently disregarded the RNAi results for *his-68* temporarily in order to check the genes to the right of 4.24 that were still within our mapping area. After performing RNAi analysis on every candidate gene between 4.24 and 4.71, however, we found that none generated an RNAi phenotype matching the *ax941* mutant phenotype (Table 4). Although *irs-2* and *npp-17* RNAi yielded dead embryos, dissection and staining did not yield a phenotype consistent with the *ax941* mutant. We concluded that *pas5251* may have shown N2 identity for the single recombinant strain not because of recombination occurring elsewhere, but because of a gene conversion event.

Figure 10. RNAi Phenotypes of T23D8.5 (*his-67*) and T23D8.6 (*his-68*)

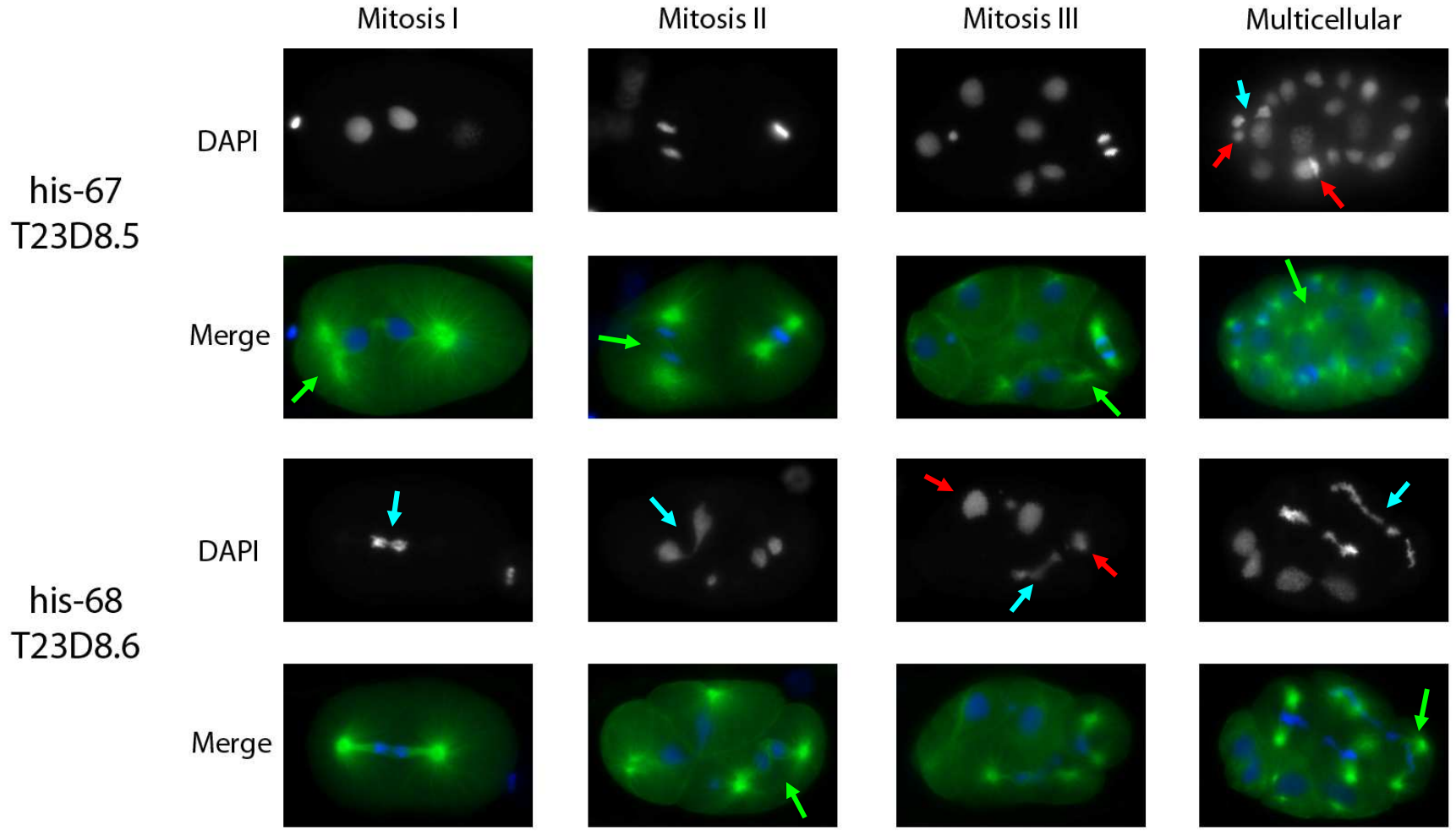

Knockdown of *his-67* and *his-68* yielded phenotypes similar to the *ax941* mutant phenotype. Whereas *his-68* knockdown caused profound and dramatic defects in chromosome segregation and tubulin structure as early as the first mitotic division, *his-67* RNAi displayed much lower penetrance and a less severe phenotype. Knockdown of *his-67* nevertheless showed aberrant tubulin patterns (green arrows) in the first several mitotic divisions, followed by DNA bridging (light blue arrows) and unequal nuclear size (red arrows) in later multicellular stages. All pictures were taken at 400X optical zoom. DNA is false-colored blue, tubulin is stained green.

According to the double Holliday junction model for homologous recombination, recombination requires the reciprocal pairing of a resected strand with a homologous strand of the opposite chromosome (Holliday 1964, Whitby 2005). As strand invasion takes place, one end of the cut strand basepairs with the homologous region on the corresponding strand, followed by reciprocal invasion by the intact strand (Figure 11). The displacement loop formed by the crossed strands requires the homologous strands to basepair with each other for a significant length until the Holliday structure breaks and resolves into the final recombination products. While chromosomal crossover is typically depicted as a clear-cut rearrangement of segments from one chromosome to another, the distinction between the two chromosomes is irreversibly blurred near the site of recombination. Since annealing between the two strands is necessary for the Holliday structure to form, any sequence differences near the crossover site will result in base mismatches that must be repaired. The DNA repair machinery cannot distinguish the original strand from the new strand, leading to the effectively random conversion of one strand to match the other. In other words, repair of DNA mismatches near the recombination site leads to non-reciprocal transfer of DNA information between the homologous strands. This so-called gene conversion can potentially erase and replace an entire allele with a copy from the other strand, but its scope is restricted to the size of the displacement loop. SNPs are single basepair sequence differences, and will thus be subject to the same mismatch repair if they fall near the recombination site. To put this hypothetical situation in scale, the map distance from the gene cluster containing *his-68* and *his-67* at 4.13 to *pas5251* at 4.24 is a scant 8.4 thousand basepairs – average gene conversion tract lengths range from several hundred base pairs to several thousand, and this tract may in turn be located some distance away from the actual site of recombination due to displacement loop movement (Hilliker *et al*. 1994, Borts *et al*.

Figure 11. Holliday Recombination Model

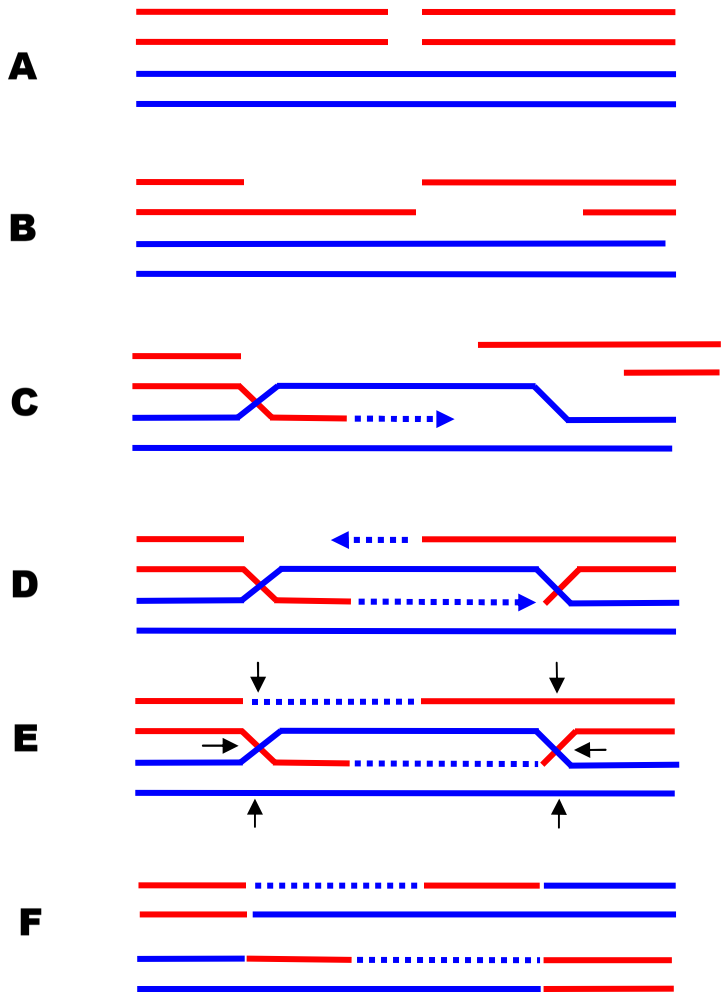

Double stranded break model for recombination. A. Double stranded break formation in one chromosome. B. Resection of DNA from break. C. Strand invasion of homologous sequence, formation of displacement loop, and beginning of DNA synthesis. D. Second strand capture, followed by DNA synthesis. E. Ligation of strands prior to cleavage of recombination structure at designated arrows. F. Crossover outcome of recombination. Note that depending on which arrows were cleaved, crossover may occur in the opposite direction. Non-crossover products are not shown. Gene conversion occurs in regions where strands from opposite chromosomes are paired, i.e. where red and blue strands are matched.

1989). If crossing over successfully replaced the *ax941* mutant gene with the wildtype allele at 4.13, *pas5251* could have plausibly been converted to the N2 variant in the same recombination event. In the face of the other SNP mapping and RNAi data, we believe that gene conversion adequately explains the presence of N2 DNA at the *pas5251* locus in that recombinant strain. We subsequently returned to studying *his-68* and its neighbor gene, *his-67*.

RNAi analysis of the histone genes *his-68* and *his-67* yielded knockdown phenotypes matching the *ax941* mutant phenotype. We performed RNAi analysis in N2 and *ax941* backgrounds at 25°C and 20°C, respectively, and found that successful knockdown of either histone caused the same DNA segregation and spindle pole defects as the *ax941* mutant (Figure 10). Consistent with reported data on Wormbase, the penetrance of RNAi in *his-67* was significantly lower than that of *his-68*, with less than 20% of embryos displaying the knockdown phenotype. The severity of the phenotype was also reduced in *his-67* RNAi compared to *his-68* RNAi and *ax941*, with bridging becoming prominent only in later mitotic divisions. Reduced penetrance and severity in no way diminishes the possibility that *his-67* could be the molecular identity of *ax941*, however, as siRNA knockdown is necessarily less effective than the actual mutation. Since *his-67* and *his-68* are the only genes that lie directly in the path of our mapping and successfully recreate the mutant phenotype upon knockdown, we concluded that the *ax941* mutation most likely exists in one of these two histones.

This finding is consistent with past research in embryogenesis. Previous work by Sonnichsen *et al*. examined the RNAi phenotypes of every gene in the *C. elegans* genome and created classifications for every observed early embryogenesis defect (Sonnichsen *et al*. 2005). One such category was sister chromatid separation ”cross-eyed” defects, in which embryonic “daughter nuclei are deformed and stay close to central cortex, [with] cytokinesis defects.” This

description fits the *ax941* phenotype perfectly, leading us to a closer examination of their data. Of the sixty-nine genes they categorized with that phenotype, the predominant groups were kinetochores, centromere-associated proteins, and histones. Of these genes, only two were located on chromosome 1 in our mapping region: *his-67* and *his-68*. These genes were also examined by Baugh *et al*. in their analysis of the early embryogenesis transcriptome, i.e. the collection of maternal and embryonic mRNA transcripts in the embryo. Both *his-67* and *his-68* were found to be present in the embryo's transcriptome: *his-68* was solely maternally deposited, while *his-67* was both maternally and embryonically expressed (Baugh *et al*. 2003). An additional difference is that whereas *his-67* has at least six paralogs also expressed maternally, *his-68* has only four (Reinke *et al*. 2000, Appendix C). This difference in expression pattern may explain why the RNAi penetrance of *his-67* was significantly lower than that of *his-68*. Since the mechanism of a ts mutant phenotype is not equivalent to sheer RNAi knockdown, the incomplete penetrance of *his-67* does not diminish the possibility of *his-67* being the molecular identity of the *ax941* mutant. By taking these past findings into account, we firmly believe we have confined the *ax941* mutant to a mutation in one of these embryogenesis-enriched histones.

A histone defect can explain the plethora of defects associated with the *ax941* mutant. The candidate genes *his-68* and *his-67* code for histone-2A (H2A) and histone-4 (H4) proteins, respectively, which are both integral parts of the core nucleosome. The nucleosome is responsible for condensing DNA into compact bundles during replication and mitosis; without nucleosomes, DNA would exist as a loosely coiled mass of strands incapable of segregating or resolving from each other. We posit that this scenario is exactly what the mutant experiences at restrictive temperatures. At 25°C, the histone folds improperly, thereby preventing the embryonic nucleosomes from assembling appropriately. With DNA unable to condense,

separation of chromosomes during anaphase is severely hampered by the tangled DNA strands, leading to slower segregation and the manifestation of DNA bridging as seen under a microscope (Figure 2). As the cell enters telophase, the midbody microtubules of the central spindle attempt to initiate the cleavage furrow for cytokinesis to occur; however, with some chromosomes still knotted together between the two nuclei, multiple scenarios can ensue. The chromosomes may incompletely separate, with small chromatin bridges connecting the two daughter cells even as cytokinesis seals off the rest of the cytoplasm (Figure 10). The chromosomes may also resolve from each other, but in an asymmetric fashion, leading to the observation of dramatically different DNA content in daughter nuclei. Another possibility occurs when the chromosomes fail to segregate into separate nuclei at all, and cytokinesis completely regresses as a result. With both centrosomes left in a single cell, any subsequent divisions will be plagued by extra centrosomes that only enhance the segregation defects. Even the onset of the mutant phenotype fits with a histone defect: with every cell division, the total number of stored maternal histones remains the same, while the DNA content doubles. At the restrictive temperature, enough functional gene products may be present to allow for a single normal mitotic division. As the daughter cells become depleted of histones, however, separating and replicating the DNA becomes more difficult, to the point that virtually all multi-cellular embryos show the most severe of the listed phenotypes. The entire *ax941* mutant phenotype can plausibly arise from a single defective histone gene.

Sequencing

With two candidate genes firmly established, we next sought to determine the molecular basis of the mutation. To this end, we sequenced *his-68* and *his-67* in the *ax941* background. Our preliminary analysis found no consistent mutations in *his-68*, but did reveal a point mutation

in the *his-67* gene that changes an alanine residue to a proline (A84P, Figure 12). Due to time constraints, we were only able to obtain two independent sequencing reads that identified this mutation; while other reads were attempted, the fidelity of the sequencing was insufficient to support or deny the mutation's identity. Since proline is an unusually rigid amino acid, the mutation of an alanine to a proline would be expected to severely disrupt the protein's structure. We therefore examined the location of this mutation in the H4 histone and the nucleosome as a whole.

Structure analysis of the putative *his-67* mutation provides a potential explanation for the temperature-sensitive phenotype. The mutated alanine is the first residue in the third α-helix of histone H4, adjacent to the DNA binding loop (Figures 13 and 14). Of all the locations for a proline substitution to occur in a histone, this site is perhaps the most innocuous: if the proline occurred in the middle of an α-helix, the histone would never fold correctly; if the proline occurred in the DNA binding loop between the α-helices, then the histone would lose the ability to bind DNA at all. A polymorphism in this site is not unprecedented, either – *Saccharomyces cerevisiae*, the model yeast species, has a serine in place of the alanine residue. A proline substitution is of course more drastic than serine, however, as its rigid ring structure severely restricts the bond angles of the protein's tertiary structure. We therefore posit that the proline substitution does not disrupt the overall tertiary structure of the histone at low temperatures, but the rigid amino acid destabilizes the protein to the point that a slight increase in temperature causes the entire structure to fall apart.

Figure 12. Sequencing Alignments

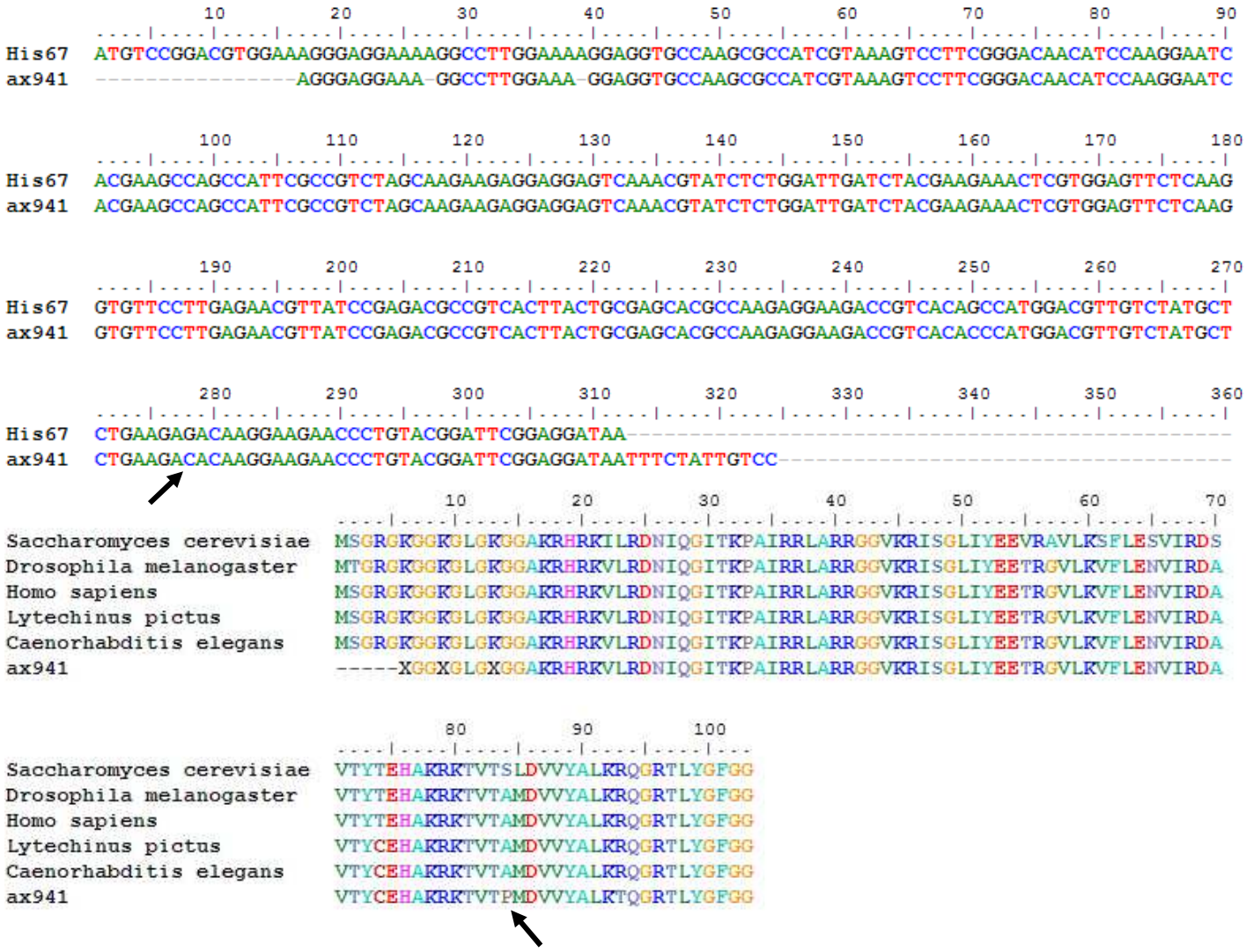

Preliminary sequencing of *his-67* yielded a potential mutation that substitutes a proline residue for alanine at site 84. Nucleotide alignment shown at top, clustal amino acid alignment shown at bottom.

Figure 13. Histone H4 in the Nucleosome

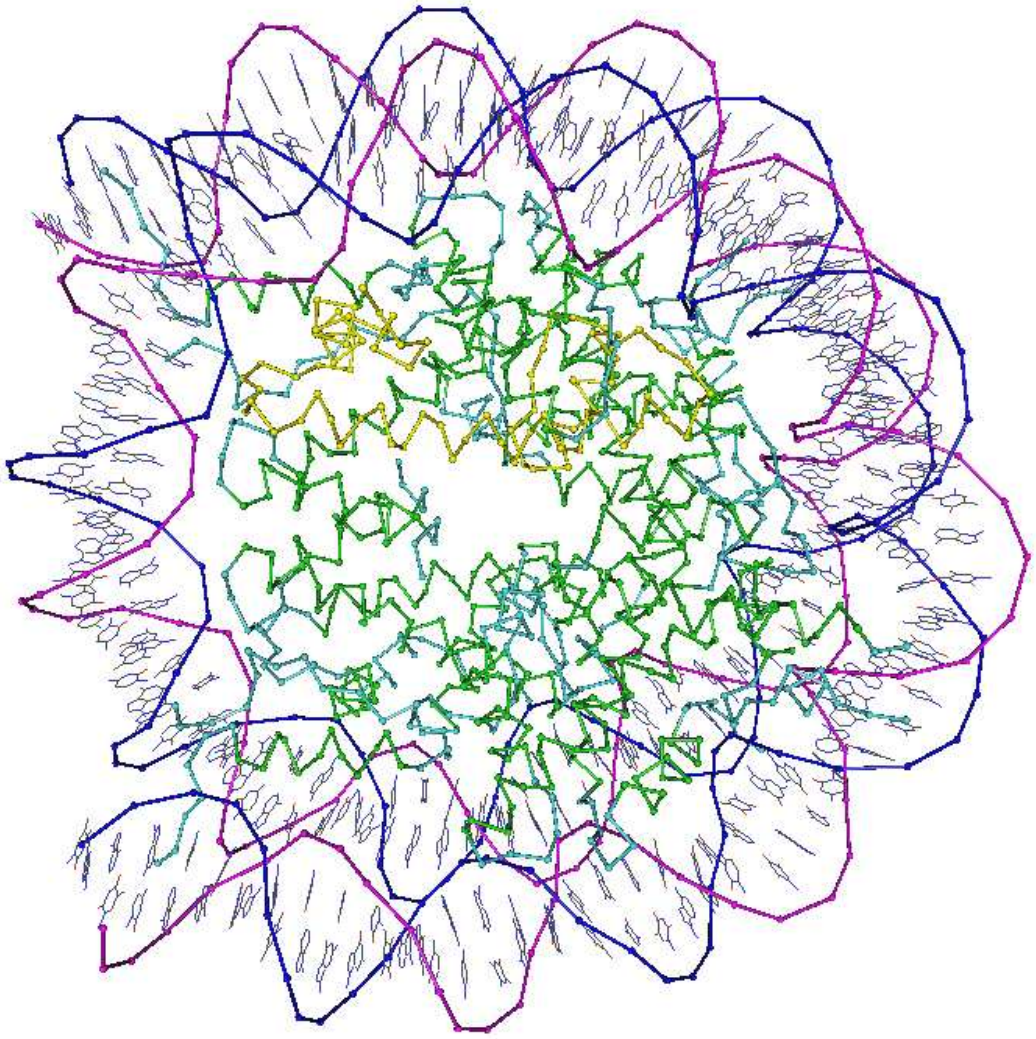

Histone H4 is denoted in yellow. H4 possesses two DNA binding loops and three α-helices that bind other histones in the core. Other histones are shown in green and teal, while DNA strands are depicted in blue and purple. This structure was adapted from nucleosome structure 2NQB, sequence B, using Cn3D.

Figure 14. Candidate Mutation in *HIS-67*

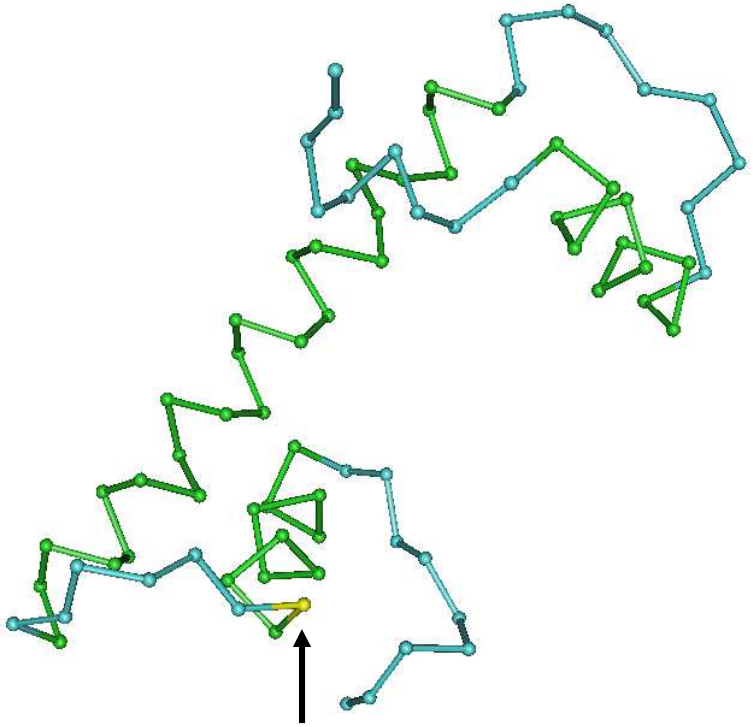

The mutated alanine residue is the first residue in the last α-helix of histone H4. Proline substitution would be expected to disrupt the stability of the histone by altering folding angles or reducing α-helix interactions in the nucleosome core. This structure was adapted from nucleosome structure 2NQB, sequence B, using Cn3D.

Discussion

Mapping Summary

Our mapping and RNAi experiments extend the phenotype analysis previously performed by Mark Astoria. In his thesis work, Astoria attributed the myriad of defects – DNA bridging, delayed segregation, and multiple spindle poles – to either a microtubule or cyclin defect. His study suffered from a lack of conclusive mapping data, however, which forced him to suggest likely gene candidates from the entire population of mitosis-related proteins. While spindles and cell cycle proteins are certainly involved in the larger scheme of mitosis affected by the *ax941* mutation, our mapping data has led us in a different direction. Two histone proteins, *his-67* and *his-68*, lie directly in the genomic area predicted by our mapping (Figure 14). Subsequent RNAi analysis of both histones produced embryonic lethal phenotypes identical to the *ax941* mutant in both N2 and *ax941* strains. Sequencing further revealed a candidate mutation in the *his-67* gene that causes a proline substitution inside the core histone. We therefore posit that the *ax941* mutant phenotype results from a mutation in a histone specific to embryogenesis, the transcripts of which are maternally deposited in the embryo.

Histone mutations have been previously reported in the scientific literature, with a range of phenotypes. Maruyama *et al*. studied three ts mutations in a core histone that ran the gamut of phenotypes: one mutation led to disrupted gene silencing, another caused delayed chromosome segregation, and another had little phenotype effect (Maruyama *et al*. 2006). Still other mutations have been shown to affect centromere formation and gene activation (Ahmed *et al*. 2007, Santisteban *et al*. 1997). In a curious twist on these mutants, a wt plant histone has been found to possess a temperature-sensitive site that mediates transcription as a temperature response (Kumar and Wigge 2010). The *ax941* mutant produces defects in chromosomal

segregation, but any effects on gene regulation are unknown. We believe that any effects on gene regulation have been hidden by the lethal phenotype during embryogenesis, and remain to be elucidated in the future.

Future Directions

Our study of the *ax941* mutant leaves many avenues open to further research. Foremost among them is confirmation of the mutation found by our sequencing. Time constraints prevented us from conducting additional sequencing reads of the two histone genes; establishing the molecular identity of the *ax941* mutant is of utmost importance for future research to be conducted. Additional independent sequencing reads revealing the mutation, ideally with different primer sets, are needed to confirm our mapping and sequencing analysis.

Assuming that the mutant indeed lies in one of the histones, then the next step would be testing the localization of the mutant proteins. GFP::Histone transgene constructs have been used in the past to stain DNA; creating such a construct for the mutant could instead allow for direct visualization of mutant histone expression and localization. This approach would be preferred over antibody staining due to the extraordinary conservation of histones across taxa and the high likelihood that an antibody would cross-react with the histone's paralogs. Of particular interest to this study is whether the mutant histone is degraded or left intact during early embryogenesis. Since non-functional copies of the histone may still interfere with normal cell function, the expression pattern would elucidate whether the ts phenotype is a simple loss-of-function or a more complicated complex poisoning event.

Although antibody staining is unlikely to reveal changes in histone localization patterns, future immunological work would help to confirm and expand on the *ax941* mutant phenotype. Staining a known histone binding partner and looking for aberrations would provide additional

evidence that *ax941* results from a histone defect and potentially increase our understanding of the mutant. Examining the kinetochores and cohesins that organize centromeres, for instance, could explain whether the lagging anaphase results from centromere separation failure or simply gross DNA entanglement. In a similar vein, analyzing the localization of histone-modifying enzymes may reveal whether epigenetic regulation is affected by the *ax941* mutant.

The effect of this mutation on gene regulation also stands to be determined. Although we classified *ax941* as a maternal effect lethal mutant, a histone defect would likely have phenotypic effects even past embryogenesis. These phenotypes would normally be hidden by the lethal nature of the mutant, but a simple change in protocol should theoretically reveal any developmental phenotypes of the mutant. Upshift experiments, in which hatched larvae are upshifted to and incubated at the restrictive temperature, would bypass the lethal stage and allow us to evaluate any larval and adult phenotypes of the *ax941* mutant. Astoria attempted one such experiment in his research, and found that L1 larva upshifted to the restrictive temperature moved sluggishly and occasionally died before reaching adulthood. Further experimentation along these lines could shed light on the expression patterns of these histones, as well as their roles in governing transcription of particular genes.

We must finally consider the possibility that the *ax941* locus is not one of the two histone genes identified by RNAi. While we are confident in our mapping data, RNAi knockdown can only translate directly into loss-of-function mutants, which may not describe the *ax941* allele. The fact that *his-67* and *his-68* RNAi matches the *ax941* phenotype may in fact be sheer coincidence, and the actual mutant gene could be elsewhere in our mapping region. To that end, further work should be performed on nearby genes, particularly those with uncharacterized RNAi phenotypes. A gene in the same operon as *his-68*, T23D8.7, has no known RNAi

phenotype, but is a paralog to Dicer-family proteins that do have embryonic lethal RNAi phenotypes. The gene product is also maternally deposited in the embryo, and expression is particularly enriched in oogenesis. If neither histone gene proves to be the source of the *ax941* allele, then T23D8.7 is a prime candidate for further examination via sequencing.

Tables

Table 1. Selected Mapping SNPs

SNP	Map Position	Nucleotide Position	Identification Type	Recombination Rate
pkP1056	0.650	5999823	SNiP-SNP	5 / 20
pkP1119	2.878	8508270	SNiP-SNP	15 / 20
pkP1061	3.912	9827852	SNiP-SNP	19 / 20
pkP1075	5.058	10614679	SNiP-SNP	20 / 20

Table 2. Additional SNPs Evaluated

SNP	Map Position	Nucleotide Position	Identification Type	Identity
pkP1123	4.001	9899924	SniP-SNP	N2
CE1-182	4.099	9958062	Sequencing	N2
pas5251	4.240	10003010	Sequencing	N2
CE1-183	4.580	10069729	Sequencing	HA

Table 3. Deficiency Breakpoints

Deficiency	Left Boundary End	Left Boundary Start	Right Boundary Start	Right Boundary End
qDf5	3.90	4.14	4.50	4.72
qDf10	3.99	4.12	4.50	4.78
mnDf111	2.08	2.40	3.76	4.50

Table 4. RNAi Targets

Gene	Name	Loc.	Emb?	Gene	Name	Loc.	Emb?
T24D1.3		4.1		F10G8.2		4.51	
T24D1.4	*tag-179*	4.1		F10G8.4	*eak-6*	4.52	
T23D8.1	*mom-5*	4.12		F10G8.3	*npp-17*	4.54	Yes
T23D8.3		4.12		F10G8.7		4.56	
T23D8.4	*eif-3C*	4.13		F10G8.5	*ncs-2*	4.56	
T23D8.9	*sys-1*	4.13		F10G8.6		4.57	
T23D8.5	*his-67*	4.13	Yes	F10G8.9		4.57	
T23D8.6	*his-68*	4.13	Yes	F10G8.8		4.57	
T23D8.7		4.14		B0379.2		4.58	
T23D8.8	*cfi-1*	4.14		B0379.7		4.59	
C03C11.1		4.45		B0379.1		4.59	
C03C11.2	*fog-3*	4.5		C25A1.5		4.71	
				C25A1.7	*Irs-2*	4.71	Yes

Appendices

Appendix A. Primers Used

Locus	Map Position	Nucleotide Position	Source	Left Primer (5'-3')	Right Primer (5'-3')	Annealing Temperature
pkP1056	I:0.650	5999823	Wormbase	AGCTCCGTAAAGCAGCTTC	CCTCGGAGGAATTTCAAACG	52°C
pkP1119	I:2.878	8508270	Wormbase	TCAAATTTGGCACGTCATCAG	CTCCATTTTGGAACTCCCAG	52°C
pkP1061	I:3.912	9827852	Wormbase	AGGGTAGCCAACACAATGAC	TTTGGATAGGTCTCGAAGCG	52°C
pkP1123	I:4.001	9899924	Wormbase	TGGGATCTCAGAAATCATCC	TTTTCGTGTTACAGCGTCC	51°C
CE1-182	I:4.099	9958062	Designed	TCGATGGCTTGTTGGTACTCT	AAAGGCCTGATTTTCCGAAT	51°C
T23D8.5	I:4.130	9988785*	Designed	CGTGAGTCTTCAGCCAATCA	GCAATCGGACTGTTTGGATT	55°C
T23D8.6	I:4.130	9989090*	Designed	TTACGATCACCAATCGCTCA	GTTCGGTGGGTTTTTGGATT	55°C
pas5251	I:4.240	10003010	Designed	GCCTCCTGGCTTCACTTCTA	GACAAACGGGGGTTTATTCA	53°C
CE1-183	I:4.580	10069729	Designed	TATCCCCACTGGGAAAGTTG	GGGCCAAATATTCTCCCATT	53°C
pkP1075	I:5.058	10614679	Wormbase	TTCACTCCAGCCGATCAATG	AGCATTTCCAGATCCGACTC	55°C

* Denotes start of gene coding sequence

Appendix B. SNP Mapping Results

Recombinant Line	Single Nucleotide Polymorphism						
	pkP1056	**pkP1119**	**pP1061**	**pkP1123**	**CE1-182**	**pas5251**	**pkP1075**
AA29	N2	HA	HA	(HA)	(HA)	(HA)	HA
DD32	HA	HA	HA	(HA)	(HA)	(HA)	HA
EE33	N2	N2	HA	(HA)	(HA)	(HA)	HA
FF34	HA	HA	HA	(HA)	(HA)	(HA)	(HA)
H8	N2	HA	HA	HA	(HA)	(HA)	HA
I9	N2	HA	HA	(HA)	(HA)	(HA)	HA
L17	HA	HA	HA	(HA)	(HA)	(HA)	HA
P20b	HA	HA	HA	(HA)	(HA)	(HA)	HA
Q22	N2	HA	(HA)	(HA)	(HA)	(HA)	HA
S14	N2	N2	HA	(HA)	(HA)	(HA)	HA
T15	N2	N2	N2	N2	N2	**N2**	HA
U24	N2	HA	HA	(HA)	(HA)	(HA)	HA
V23	HA	HA	HA	(HA)	(HA)	(HA)	HA
Z27	N2	HA	HA	(HA)	(HA)	(HA)	HA
R0	N2	N2	HA	(HA)	(HA)	(HA)	HA
R3	N2	HA	HA	(HA)	(HA)	(HA)	HA
R6	N2	HA	HA	(HA)	(HA)	(HA)	HA
R10	N2	N2	HA	(HA)	(HA)	(HA)	HA
R11	N2	HA	HA	(HA)	(HA)	(HA)	HA
R12	N2	HA	HA	(HA)	(HA)	(HA)	HA

Parentheses denote identities extrapolated from existing data. Bolded data represents a presumed gene conversion event.

Appendix C. *his-67* and *his-68* Paralogs

his-67 Paralogs	Expression	his-68 Paralogs	Expression
his-56	Uncharacterized	his-33	Strictly Embryonic
his-31	Embryonic and Maternal	his-65	Uncharacterized
his-5	Embryonic and Maternal	his-51	Uncharacterized
his-14	Uncharacterized	his-16	Uncharacterized
his-50	Muscle-Depleted	his-12	Embryonic and Maternal
his-28	Uncharacterized	his-57	Uncharacterized
his-18	Muscle-Depleted	his-47	Embryonic and Maternal
his-1	Strictly Embryonic	his-21	Uncharacterized
his-46	Embryonic and Maternal	his-53	Uncharacterized
his-10	Embryonic and Maternal	his-7	Embryonic and Maternal
his-26	Uncharacterized	his-61	Embryonic and Maternal
his-38	Embryonic and Maternal	his-30	Uncharacterized
his-64	Muscle-Depleted	his-3	Strictly Embryonic
his-37	Embryonic and Maternal, Starved Arrest	his-19	Uncharacterized
his-60	Early Larval Development	his-43	Uncharacterized

Acknowledgements

- The Monroe Scholars program, for providing summer research funding.
- The Jeffress Memorial Trust, for funding the lab's research grant.
- Marc Presler, Brian Neva, Leah Towarnicky, Kishan Patel, Zach Dillingham, my fellow lab workers and colleagues, for their support and encouragement.
- Katie Guevel, my lab partner, for her overwhelming patience and cheer.
- Dr. Glenn Harris and Lataissia Jones, our collaborators at Virginia State University, who performed the initial SNP mapping from the opposite direction.
- Dr. Aurora Kerscher, for graciously providing RNAi lines.
- Dr. Penny Sadler, for her tremendous expertise and advice over the years.
- Dr. Shakes, for gently correcting my mistakes, continually inspiring me in science, and never ceasing to serve as a role model in scholarship and conduct.

- **References**

1. Ahmed, S., Dul, B., Qiu, Xinxing, and Walworth, N.C. Msc1 Acts Through Histone H2A.Z to Promote Chromosome Stability in *Schizosaccharomyces pombe*. Genetics *177*, 1487-1497 (2007).
2. Akam, M. The molecular basis for metameric pattern in the *Drosophila* embryo. Development *101*, 1-22 (1987).
3. Allshire, R.C., and Karpen, G.H. Epigenetic regulation of centromeric chromatin: old dogs, new tricks? Nature Reviews Genetics *9*, 923-937 (2008).
4. Altschul, S.F., Madden, T.L., Schaffer, A.A., Zhang, J., Zhang, Z., Miller, W., Lipman, D.J. Gapped BLAST and PSI-BLAST: a new generation of protein database search programs. Nucleic Acids Research *25*, 3389-3402 (1997).
5. Baugh, L.R., Hill, A.A., Slonim, D.K., Brown, E.L., and Hunter, C.P. Composition and dynamics of the *Caenorhabditis elegans* early embryonic transcriptome. Development *130*, 889-900 (2003).
6. Borts, R.H., and Haber, J.E. Length and Distribution of Meiotic Gene Conversion Tracts and Crossovers in *Saccharomyces cerevisiae*. Genetics *123*, 69-80 (1989).
7. Bowerman, B. Maternal control of pattern formation in early *Caenorhabditis elegans* embryos. Current Topics in Developmental Biology *39*, 73-117 (1998).
8. Boyd, L., Guo, S., Levitan, D., Stinchcomb, D.T., and Kemphues, K.J. PAR-2 is asymmetrically distributed and promotes association of P granules and PAR-1 with the cortex in *C. elegans* embryos. Development *122*, 3075-3084 (1996).
9. Brenner, S. The genetics of *Caenorhabditis elegans*. Genetics *77*, 71-94 (1974).

10. Campos, E.I., and Reinberg, D. Histones: annotating chromatin. Annual Review of Genetics *43*, 559-599 (2009).

11. Dai, F., Yu, L., He, H., Zhao, Y., Yang, J., Zhang, X., and Zhao, S. Cloning and mapping of a novel human serum/glucocorticoid regulated kinase-like gene, SGKL, to chromosome 8q12.3-q13.1. Genomics *62*, 95-97 (1999).

12. Davis, M.W., and Hammarlund, M. Single-nucleotide polymorphism mapping. Methods in Molecular Biology *351*, 75-92 (2006).

13. De Clercq, A., and Inze, D. Cyclin-dependent kinase inhibitors in yeast, animals, and plants: a functional comparison. Critical Reviews in Biochemistry and Molecular Biology *41*, 293-313 (2006).

14. Doxsey, S., Zimmerman, W., and Mikule, K. Centrosome control of the cell cycle. Trends in Cell Biology *15*, 303-311 (2005).

15. Fay, D. Genetic mapping and manipulation: Chapter 5-SNPs: Three-point mapping. *WormBook*, http://www.wormbook.org/ (2006).

16. Fire, A., Xu, S., Montgomery, M.K., Kostas, S.A., Driver, S.E., and Mello, C.C. Potent and specific genetic interference by double-stranded RNA in *Caenorhabditis elegans*. Nature *391*, 806-811 (1998).

17. Fraser, A.G., Kamath, R.S., Zipperlen, P., Martinez-Campos, M., Sohrmann, M., and Ahringer, J. Functional genomic analysis of *C. elegans* chromosome I by systematic RNA interference. Nature *408*, 325-330 (2000).

18. Glowczewski, L., Yang, P., Kalashnikova, T., Santisteban, M.S., and Smith, M.M. Histone-Histone Interactions and Centromere Function. Molecular and Cellular Biology *20*, 5700-5711 (2000).

19. Grunstein, M. Histone acetylation in chromatin structure and transcription. Nature *389*, 349-352 (1997).

20. Hasimoto H., Takami Y., Sonoda E., Iwasaki T., Iwano H., Tachibana M., Takeda S., Nakayama T., Kimura H., and Shinkai Y. Histone H1 null vertebrate cells exhibit altered nucleosome architecture. Nucleic Acids Research *Epub* (2010).

21. Hilliker, A.J., Harauz, G., Reaume, A.G., Gray, M., Clark, S.H., and Chovnick, A. Meiotic Gene Conversion Tract Length Distribution Within the *rosy* locus of *Drosophila melanogaster*. Genetics *137*, 1019-1026 (1994).

22. Ho, L., and Crabtree, G. R. Chromatin remodeling during development. Nature *463*, 474-484 (2010).

23. Holliday, R. A mechanism for gene conversion in fungi. Genetical Research *5*, 282-304 (1964).

24. Iovine, M.K., and Johnson, S.L. A genetic, deletion, physical, and human homology map of the long fin region on zebrafish linkage group 2. Genomics *79*, 756-79 (2002).

25. Kornberg, R.D. Chromatin structure: a repeating unit of histones and DNA. Science *184*, 868–871 (1974).

26. Kumar, S.V., and Wigge, P.A. H2A.Z-containing nucleosomes mediate the thermosensory response in *Arabidopsis*. Cell *140*, 26-28 (2010).

27. Lim, L.P., Lau, N.C., Weinstein, E.G., Abdelhakim, A., Yekta, S., Rhoades, M.W., Burge, C.B., and Bartel, D.P. The microRNAs of *Caenorhabditis elegans*. Genes and Development *17*, 991-1008 (2003).

28. Luger, K., Mader, A.W., Richmond, r.K., Sargent, D.F., and Richmond, T.J. Crystal structure of the nucleosome core particle at 2.8 Å resolution. Nature *389*, 251-260 (1997).

29. Maine, E.M. Studying gene function in *Caenorhabditis elegans* using RNA-mediated interference. Briefings in Functional Genomics & Proteomics *7*, 184-194 (2008).

30. Maruyama, T., Nakamura, T., Hayashi, T., and Yanagida, M. Histone H2B mutations in inner region affect ubiquitination, centromere function, silencing and chromosome segregation. The EMBO Journal *25*, 2420-2431 (2006).

31. McKim, K.S., Starr, T., and Rose, A.M. Genetic and molecular analysis of the *dpy-14* region in *Caenorhabditis elegans*. Molecular and General Genetics *233*, 241-251 (1992).

32. Pushparaj, P.N., Aarthi, J.J., Manikandan, J., and Kumar, S.D. siRNA, miRNA, and shRNA: *in vivo* applications. Journal of Dental Research *87*, 992-1003 (2008).

33. Reinke, V., Smith, H.E., Nance, J., Wang, J., Doren, C.V., Begley, R., Jones, S.J.M., Davis, E.B., Scherer, S., Ward, S., and Kim, S.K. A Global Profile of Germline Gene Expression in *C. elegans*. Molecular Cell *6*, 605-616 (2000).

34. Santisteban, M.S., Arents, G., Moudrianakis, E.N., and Smith, M.M. Histone octamer function *in vivo*: mutations in the dimer-tetramer interfaces disrupt both gene activation and repression. The EMBO Journal *16*, 2493-2506 (1997).

35. Sigurdson, D.C., Spanier, G.J., and Herman, R.K. *Caenorhabditis elegans* deficiency mapping. Genetics *108*, 331-345 (1984).

36. Simpson, V.J., Johnson, T.E., and Hammen, R.F. *Caenorhabditis elegans* DNA does not contain 5-methylcytosine at any time during development. Nucleic Acids Research *14*, 6711–6719 (1986).

37. Sonnichsen, B., Koski, L.B., Walsh, A., Marschall, P., Neumann, B., Brehm, M., Alleaume, A.M., Artelt, J., Betterncourt, P., Cassin, E., Hewitson, M., Holz, C., Khan, M., Lazik, S., Martin, C., Nitzsche, B., Ruer, M., Stamford, J., Winzi, M., Heinkel, R., Roder, M., Finell, J.,

Hantsch, H., Jones S.J.M., Jones, M., Piano, F., Gunsalus, K.C., Oegema, K., Gonczy, P., Coulson, A., Hyman, A.A., and Echeverri C.J. Full-genome RNAi profiling of early embryogenesis in *Caenorhabditis elegans*. Nature *434*, 462-469 (2005).

38. Thacker, C., Sheps, J.A., Rose, A.M. *Caenorhabditis elegans dpy-5* is a cuticle procollagen processed by a proprotein convertase. Cellular and Molecular Life Sciences *63*, 1193-1204 (2006).
39. Timmons, L., and Fire, A. Specific interference by ingested dsRNA. Nature *395*, 854 (1998).
40. Updike, D.L., and Mango, S.E. Temporal regulation of foregut development by HTZ-1/H2A.Z and PHA-4/FoxA. PLoS Genetics *2*, e161 (2006).
41. Walczak, C.E., Cai, S., and Khodjakov, A. Mechanisms of chromosome behaviour during mitosis. Nature Reviews Molecular Cell Biology *11*, 91-102 (2010).
42. Whitby, M.C. Making crossovers during meiosis. Biochemical Society Transactions *33*, 1451-1455 (2005).
43. Wilkinson K.D. Protein ubiquitination: a regulatory post-translational modification. Anticancer Drug Design *2*, 211-229 (1987).
44. Xu, D., Bai, J., Duan, Q., Costa, M., and Dai, W. Covalent modifications of histone during mitosis and meiosis. Cell Cyle *8*, 3688-3694 (2009).